CONDUCTIVE INKJET PRINTED ANTENNAS ON FLEXIBLE LOW-COST PAPER-BASED SUBSTRATES FOR RFID AND WSN APPLICATIONS

A Thesis
Presented to
The Academic Faculty

By

Amin H. Rida

In Partial Fulfillment
Of the Requirements for the Degree
Master of Science in the School of Electrical and Computer Engineering

Georgia Institute of Technology

May 2009

CONDUCTIVE INKJET PRINTED ANTENNAS ON FLEXIBLE LOW-COST PAPER-BASED SUBSTRATES FOR RFID AND WSN APPLICATIONS

Approved by:

Dr. Emmanouil M. Tentzeris, Advisor
School of Electrical and Computer
Engineering
Georgia Institute of Technology
Dr. Joy Laskar
School of Electrical and Computer
Engineering
Georgia Institute of Technology
Dr. Gregory Durgin
School of Electrical and Computer
Engineering
Georgia Institute of Technology
 Date Approved: 3/17/2009

ACKNOWLEDGEMENTS

TABLE OF CONTENTS

LIST OF TABLES

LIST OF FIGURES

LIST OF SYMBOLS AND ABBREVIATIONS

RF   Radio Frequency

RFID   Radio Frequency Identification

IC   Integrated Circuit

ε_r dielectric constant

$\tan\delta$ dielectric loss tangent

LCP   Liquid Crystal Polymer

RL   Return Loss

UHF   Ultra High Frequency

SUMMARY

This thesis investigates inkjet-printed flexible antennas fabricated on paper substrates as a system-level solution for ultra-low-cost and mass production of RF structures. These modules are designed for the UHF Radio Frequency Identification (RFID) Tags and Wireless Sensor Nodes (WSN); however the approach could be easily extended to other microwave and wireless applications.

Chapter 1 serves as an introduction to RFID technology and its capabilities while listing the major challenges that could potentially hinder RFID practical implementation.

Chapter 2 discusses the benefits of using paper as a substrate for high-frequency applications, reporting its very good electrical/dielectric performance up to at least 1 GHz. The dielectric properties are studied by using the microstrip ring resonator. Brief discussion on Liquid Crystal Polymer (LCP) is also given in this chapter.

Chapter 3 gives details about the inkjet printing technology, including the characterization of the conductive ink, which consists of nano-silver-particles, while highlighting the importance of this technology as a fast and simple fabrication technique especially on flexible organic (e.g.LCP) or paper-based substrates.

Chapter 4 focuses on antenna designs. Four examples are given to provide: i) matching techniques to complex IC impedance, ii) proof of concept of inkjet printing on paper substrate through measurement results, iii) demonstration of a fully-integrated wireless sensor modules on paper and show a 2D sensor integration with an RFID tag module on paper.

Chapter 5 concludes the thesis by explaining the importance of this work in creating a first step towards an environmentally friendly generation of "green" RF electronics and modules.

CHAPTER 1

INTRODUCTION

RFID is an emerging compact wireless technology for the identification of objects, and is considered as an eminent candidate for the realization of completely ubiquitous "ad-hoc" wireless networks. RFID utilizes electromagnetic waves for transmitting and receiving information stored in a tag or transponder to/from a reader. This technology has several benefits over the conventional ways of identification, such as higher read range, faster data transfer, the ability of RFID tags to be embedded within objects, no requirement of line of sight, and the ability to read a massive amount of tags simultaneously [1]. A listing of applications that currently use RFID are: retail supply chain, military supply chain, pharmaceutical tracking and management, access control, sensing and metering application, parcel and document tracking, automatic payment solutions, asset tracking, real time location systems (RTLS), automatic vehicle identification, and livestock or pet tracking.

The demand for flexible RFID tags has recently increased tremendously due to the requirements of automatic identification/tracking/monitoring in the various areas listed above. Compared with the lower frequency tags (LF and HF bands) already suffering from limited read range (1-2 feet), RFID tags in UHF band see the widest use due to their higher read range (over 10 feet) and higher data transfer rate [2]. The major challenges that could potentially hinder RFID practical implementation are: 1) Cost; in order for RFID technology to realize a completely ubiquitous network, the cost of the RFID tags have to be extremely inexpensive in order to be realized in mass production amounts 2) Reliability; and that extends to primarily the efficiency of the RFID tag antennas, readers, and the middleware deployed, 3) Regulatory Situation; meaning tags

1

have to abide to a certain global regulatory set of requirements, such as the bandwidth allocations of the Gen2 Protocols defined by the EPC Global regulatory unit [3] and 4) Environmentally-friendly materials, in order to allow for the easy disposal of a massive number (in the billions) of RFID tags.

This thesis demonstrates how inkjet-printing of antennas/matching networks on low-cost paper-based materials can tackle all four challenges enabling the easy implementation of ubiquitous RFID and WSN networks. It starts by discussing why paper should be used as a substrate for UHF/wireless inlays, followed by the dielectric characterization of paper using a microstrip ring resonator method. This thesis then shows how we can use conductive inkjet-printing technology for the fast fabrication of RF/wireless circuits, provides design guidelines for inkjet-printed antennas for UHF RFID tags which can be used globally, and eventually shows the capability of integrating sensors with RFID tags and discusses how this added functionality could revolutionize data fusion and real-time environmental cognition.

CHAPTER 2

FLEXIBLE ORGANIC LOW COST SUBSTRATES

2.1 Paper: The Ultimate Solution for Lowest Cost Environmental Friendly RF Substrate

There are many aspects of paper that make it an excellent candidate for an extremely low-cost substrate for RFID and other RF applications. Paper; an organic-based substrate, is widely available; the high demand and the mass production of paper make it the cheapest material ever made. From a manufacturing point of view, paper is well suited for reel-to-reel processing, as shown in Figure 1, thus mass fabricating RFID inlays on paper becomes more feasible. Paper also has low surface profile and, with appropriate coating, it is suitable for fast printing processes such as direct write methodologies instead of the traditional metal etching techniques. A fast process, like inkjet printing, can be used efficiently to print electronics on/in paper substrates. This also enables components such as: antennas, IC, memory, batteries and/or sensors to be easily embedded in/on paper modules. In addition, paper can be made hydrophobic as shown in Figure 2, and/or fire-retardant by adding certain textiles to it, which easily resolve any moisture absorbing issues that fiber-based materials such as paper suffer from [4]. Last, but not least, paper is one of the most environmentally-friendly materials and the proposed approach could potentially set the foundation for the first generation of truly "green" RF electronics and modules.

However; due to the wide availability of different types of paper that varies in density, coating, thickness, and texture, dielectric properties: dielectric constant and dielectric loss tangent, or dielectric RF characterization of paper substrates becomes an essential step before any RF "on-paper" designs. The electrical characterization of paper

need to be performed and results have shown the feasibility of the use of paper in the UHF and RF frequencies.

Another note to mention here is that the low cost fabrication and even the assembly with PCB compatible processes can realize paper boards similar to printed wiring boards, which can support passives, wirings, RFID, sensors, and other components in a 3D multi-layer platform [5-10].

Figure 1. Reels of paper.
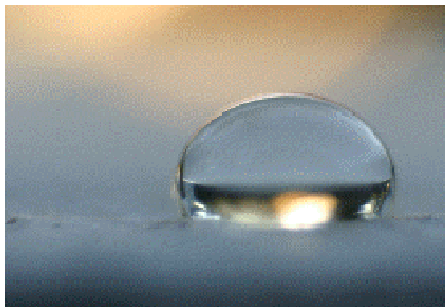
Figure 2. Magnified droplet of water sitting on a paper substrate.

2.2 Dielectric Characterization of the paper substrate

RF characterization of paper becomes a critical step for the qualification of the paper material for a wide range of frequency domain applications. The knowledge of the dielectric properties such as dielectric constant (ε_r) and loss tangent (tanδ) become necessary for the design of any high frequency structure such as RFID antennas on the paper substrate and more importantly if it is to be embedded inside the substrate. Precise methods for high-frequency dielectric characterization include microstrip ring resonators, parallel plate resonators, and cavity resonators [13]. In an extensive literature review, such properties were not found to be available for paper for the desired application frequency range (above 900 MHz).

In order to measure the dielectric constant (ε_r) and loss tangent (tanδ) of paper up to 2 GHz, a microstrip ring resonator structure was designed; the configuration diagram is shown in Figure 3. A calibration method namely through-reflect-lines (TRL) was utilized to de-embed the effect of the feeding lines. It is to be noted that tanδ extraction using the microstrip ring resonator approach requires reliable theoretical equations for the estimation of the conductor losses [2,12,13].

Among the critical needs for the selection of the right type of paper for electronics applications are the surface planarity, water-repelling, lamination capability for 3D module development, via-forming ability, adhesion, and co-processability with low-cost manufacturing. For the trial runs, a commercially available paper with hydrophobic coating was selected. The thickness of the single sheet of paper is 260±3um. An 18um thick copper foil was selected as the metallic material heat-bonded on both sides of the paper substrate, in order to accurately model and de-embed the conductive loss of the microstrip circuit. The photolithography process was conducted using a dry film photo-

5

resist followed by UV exposure and finally etching copper using a slow etching methodology. The paper substrate was then dried at 100°C for 30 minutes.

To investigate the sensitivity of the results to the paper thickness as well as to investigate the effect of the bonding process, 9 sheets of paper were directly heat-bonded together to grow a thickness of 2.3 mm, without any extra adhesive layers.

The characterization covers the UHF RFID frequency band that is utilized by applications that are commonly used in port security, inventory tracking, airport security and baggage control, automotive and pharmaceutical/healthcare industries.

The ring resonator produces Insertion Loss (S_{21}) results with periodic frequency resonances. In this method, ε can be extracted from the location of the resonances of a given radius ring resonator while $\tan\delta$ is extracted from the quality factor (Q) of the resonance peaks along with the theoretical calculations of the conductor losses. Measurements of S_{21} were done over the frequency range 0.4 GHz to 1.9 GHz using Agilent 8530A Vector Network Analyzer (VNA). Typical SMA coaxial connectors were used to feed the ring resonator structure. TRL calibration was performed to de-embed the input and output microstrip feeding lines effects and eliminate any impedance mismatch.
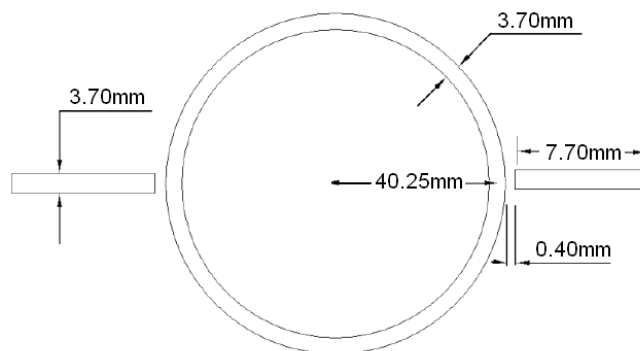
Figure 3. Microstrip ring resonator configuration diagram.

6
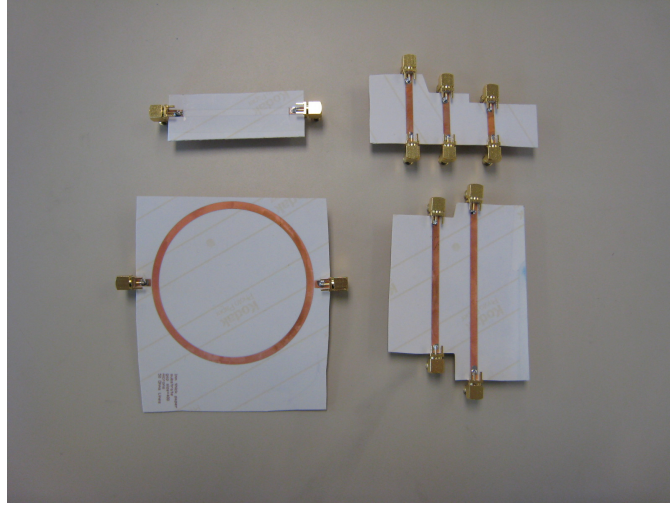
Figure 4. Photo of fabricated Microstrip ring resonators and TRL lines bonded to SMA connectors.

Figure 3 shows a layout of the ring resonator along with the dimensions for the microstrip feeding lines, the gap in between the microstrip lines and the microstrip ring resonator, the width of the signal lines, and the mean radius r_m. Figure 4 shows fabricated ring resonators with the TRL lines. S_{21} magnitude vs. frequency data were then inserted in a Mathcad program and the dielectric constant and loss tangent were extracted [5, 7, 11]. A plot of S_{21} vs. frequency is shown in Figure 5.

2.2.1 Dielectric Constant Measurements

In order to extract the dielectric constant, the desired resonant peaks were first obtained according to [5, 11]:

$$f_o = \frac{nc}{2\pi r_m \sqrt{\varepsilon_{eff}}} \tag{1}$$

where f_o corresponds to the nth resonance frequency of the ring with a mean radius of r_m and effective dielectric constant ε_{eff} with c being the speed of light in vacuum. The extracted ε_r value at 0.71 GHz and 1.44 GHz of Figure 5 was obtained using equation 1 and is shown in Table 1.
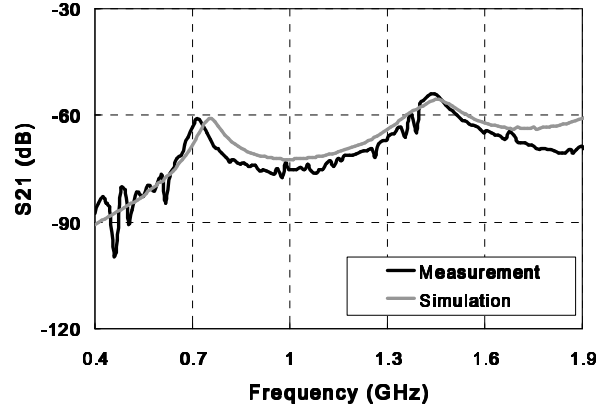
Figure 5. S_{21} vs. frequency for the ring resonator

2.2.2 Dielectric Loss Tangent Measurements

The extraction of loss tangent was performed by calculating the theoretical values of conductor and radiation losses. This is done in order to isolate the dielectric loss α_d since the ring resonator method gives the total loss at the frequency locations of the resonant peaks. The loss tangent is a function of α_d (in Nepers/m) according to [13]:

$$\tan \delta = \frac{\alpha_d \alpha_o \sqrt{\varepsilon_{eff}\left(\varepsilon_r - 1\right)}}{\pi \varepsilon_r \left(\varepsilon_{eff} - 1\right)} \tag{2}$$

where λ_o is the free-space wavelength, ε_r and ε_{eff} are the same as described above.

Available theoretical methods for calculating conductor loss and radiation loss have been dated from the 1970s [13]. Tanδ results are shown in Table 1 after subtracting the calculated conductor and radiation losses.

It is to be noted that the density of the paper substrate slightly increases after the bonding process described above [5,9]. This may slightly increase the calculated dielectric properties in Table 1 for multilayer paper-based RF modules.

8

Table 1. Extraction of dielectric constant from Ring Resonator Measurement

Mode	Resonant Freq (f_o)	Insertion Loss ($|S_{21}|$)	BW$_{-3dB}$	ε_r	tanδ
n=1	0.71 GHz	-61.03 dB	42.12 MHz	3.28	0.061
n=2	1.44 GHz	-53.92 dB	75.47 MHz	3.20	0.053

2.3 Liquid Crystal Polymer: Properties and benefits for RF Applications

Liquid Crystal Polymer (LCP) possesses attractive qualities as a high performance low-cost substrate and as a packaging material for numerous applications such as RFID/WSN modules, antenna arrays, microwave filters, high Q-inductors, RF MEMs and other applications extending throughout the mm-wave frequency spectrum. Furthermore LCP has low loss, flexible, near hermetic nature, thermal stability, low cost and controlled CTE in x-y direction make it one of the best candidates as a substrate for System on Package (SOP) approach for 3D integrated RF and mm-wave functions and modules.

The dielectric characterization of LCP substrate has been performed up to 110 GHz using several methods that are regarded as highly accurate and include: ring resonator, cavity resonator, as well as a transmission line TL method [13]. The dielectric constant vs. frequency show a value for $\varepsilon_r = 3.16 \pm 0.05$ and the tanδ was calculated to be <0.0049. This proves the excellence of LCP in electrical properties for mm-waves.

LCP also possesses numerous exceptional mechanical properties not to mention that it's an environmental friendly material. One particular example and which is of high interest in mm-wave is the coefficient of thermal expansion (CTE). LCP can be engineered to have an x-y CTE between 0 ppm/°C and 40 ppm/°C and so this unique process can achieve a thermal expansion match in the x-y plane with many commonly

used material such as Cu (16.8 ppm/°C), Au (14.3 ppm/°C), Si (4.2 ppm/°C), GaAs (5.8 ppm/°C), and SiGe (3.4-5 ppm/°C). On the other hand the z-axis CTE is considerably high (~105 ppm/°C); however and due to the fabrication miniaturization capabilities and LCP productions thin layers of LCP (2 mils LCP and 1 mil LCP bond ply), the z-expansion becomes of a minimal concern unless thick multilayer modules come into consideration. Another key capability for many applications in RF is the assumed ability of flexibility and light weight, for examples antennas on LCP may be conformed into specific shapes desired by the application needs. LCP is also a near hermetic, low water permeability. Thermal stability results have also been obtained and LCP has been proven to be as good as or better than the 10 GHz PTFE/glass and alumina temperature stability values[13]. This verifies the superiority of using this material for RF and mm-wave integrated modules, SOP, or packaging.

2.4 Summary

In summary, the choice of the substrate will depend greatly on the application. As seen in this chapter both paper and LCP can be used as low cost substrates for UHF regions, with paper being the cheapest. However, as we go up in frequency, paper's substrate loss becomes significant, and the choice is limited to LCP (and/or other low loss organic substrates) especially that LCP has several other excellent characteristics for higher frequency RF applications.

CHAPTER 3

CONDUCTIVE INK-JET PRINTING RF MODULES

3.1 Conductive Ink-jet Printing Technique

Modern inkjet printers operate by propelling tiny droplets of liquid down to several pL [14, 18]. This new technology of inkjet printing [16,18,24] utilizing conductive paste may rapidly fabricate prototype circuits without iterations in photolithographic mask design or traditional etching techniques that have been widely used in industry. Printing is completely controlled from the designer's computer and does not require a clean room environment [13]. A droplet's volume determines the resolution of the printer, for e.g. a droplet of 10 pL gives ~ 25μm minimum thickness or gap size of printed traces/lines. The cartridge consists of a Piezo-driven jetting device with integrated reservoir and heater [14, 17].

A detailed description of the Inkjet printer used for this is shown in Figure 6. The inkjet-printing is done in a horizontal bar-by-bar printing using a print-head or cartridge "DMC-11610" which has a drop volume of 10 pL nominal.

Inkjet Printing; unlike etching which is a subtractive method by removing unwanted metal from the substrate surface, jets the single ink droplet from the nozzle to the desired position, therefore, no waste is created, resulting in an economical fabrication solution. Silver nano-particle inks are usually selected in the inkjet-printing process to ensure a good metal conductivity. After the silver nano-particle droplet is driven through the nozzle, sintering process is found to be necessary to remove excess solvent and to remove material impurities from the depositions. Sintering process also provides the secondary benefit of increasing the bond of the deposition with the paper substrate [15].

The savings in fabrication/prototyping time that inkjet printing brings to RF/wireless circuits is very critical to the ever changing electronics market of today's, verifying its feasibility as an excellent prototyping and mass-production technology for next generation electronics especially in RFID, wireless sensors, handheld wireless devices (e.g.4G/4.5G cell phones), flex circuits, and even in thin-film batteries [29, 31].
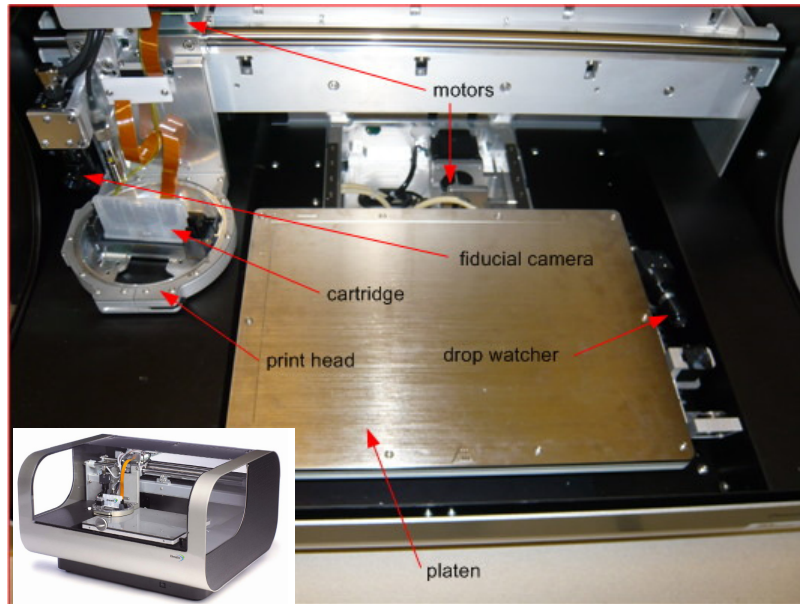
Figure 6. Details of Dimatix Material Printer DMP 2800

3.2 Curing of conductive Ink

After the printing of the antenna it is essential to cure the prototype in order to increase the conductivity of the silver ink. Curing is simply done by heating the fabricated antenna, so that the printed silver ink nano-particles melt and a good percolation channel is created for electrons to flow. The curing is performed in a high precision industrial oven, shown in Figure 7, at a constant temperature of 100°C for 10 hours. The curing must be performed immediately after the printing, because the silver ink begins to oxidize which may result into permanent poor conductivity and efficiency of the antenna trace. It has to be noted that the maximum temperature that paper can endure is 150°C.

Figure 7. Test Equity FS series industrial oven for performing curing of the prototype antenna

The conductivity of the conductive ink varies from $0.4 \sim 2.5 \times 10^7$ Siemens/m depending on the curing temperature and duration time. Figure 8 shows the difference between heating temperature 100°C and 150°C after a 15 minutes curing. At lower temperature, larger gaps exist between the particles, resulting in a poor connection. When the temperature is increased, the particles begin to expand and gaps start to diminish. That guarantees a virtually continuous metal conductor, providing a good percolation channel for the conduction electrons to flow. To ensure the conductivity performance of microwave circuits, such as RFID modules, curing temperatures around 120°C and duration time of two hours were chosen in the following fabrication to sufficiently cure the nano-particle ink. Alternatively, much shorter (within seconds) UV heating approaches can achieve similar results.
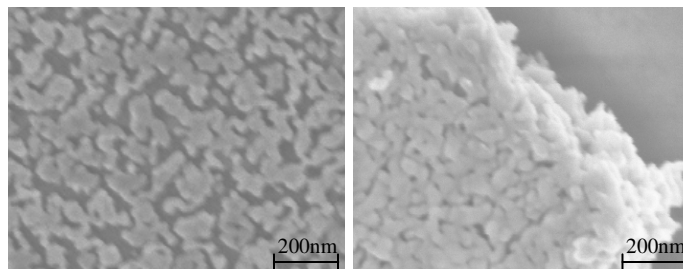
Figure 8. SEM images of a layer of printed silver nano-particle ink, after a 15 minutes curing at 100°C (left) and 150°C (right).

CHAPTER 4

BENCHMARKING PROTOTYPES

4.1 RFID antenna design challenges

A major challenge in RFID antenna designs is the impedance matching of the antenna (Z_{ANT}) to that of the IC (Z_{IC}). For years, antennas have been designed primarily to match either 50 Ω or 75 Ω loads. However, RFID chips primarily exhibit complex input impedance, making matching extremely challenging [1].

It is to be noted that besides impedance matching, low cost, omnidirectional radiation pattern, long read range, wide bandwidth, flexibility, and miniaturized size are all important features that an RFID tag must acquire. Most available commercial RFID tags are passive due to cost and fabrication requirements. A purely passive RFID system utilizes the EM power transmitted by the reader antenna in order to power up the IC of the RFID tag and transmit back its information to the reader using the backscatter phenomena. A block diagram of a passive RFID tag is shown in the Figure 9 below. The antenna matching network must provide the maximum power delivered to the IC which is used to store the data that is transmitted to/received from the reader.
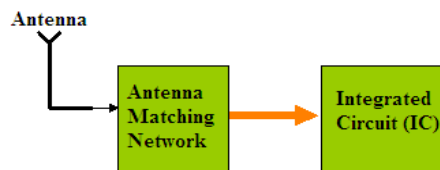
Figure 9. Block diagram of a passive RFID tag.

For a truly global operation of passive UHF RFID's, Gen2 protocols define different sets of frequency, power levels, numbers of channel and sideband spurious limits of the RFID readers signal, for different regions of operation (North America 902-

928MHz, Europe 866-868MHz, Japan 950-956MHz, and China 840.25MHz-844.75 and 920.85MHz-924.75MHz). This places a demand for the design of RFID tags that operate at all those frequencies, thus requiring a miniaturized broadband UHF antenna. For instance, in a scenario where cargo/containers get imported/exported from different regions of the world in a secured RFID system implementation, an RFID tag is required to have a bandwidth wide enough to operate globally. This imposes very stringent design challenges on the antenna designers.

4.2 RFID Antenna with Serial Stub Feeding Structures

4.2.1 Design Approach

In this design approach, a compact configuration (in an area less than 3" x 3") of a $\lambda/2$ dipole antenna was developed, where λ is the free space wavelength. The antenna design is favorable for its quasi-omnidirectional radiation pattern. The step by step design is illustrated in the figures below. Figure 10 shows the main radiating element which if stretched from one end to the other corresponds to a length of ~16cm (which is $\lambda/2$ around the center frequency 935 MHz in air). The tapering of the antenna was chosen for maximum current flow (hence optimum efficiency) and to achieve a high bandwidth. The $\lambda/2$ antenna was folded as shown in Figure 10 at a distance (~0.16 λ) not to cause any significant current perturbation, while making the design more compact. Without loss of generality, in this design the overall matching network is designed to conjugately match an RFID chip with a high capacitive impedance of Z_{IC}=73-j113 Ω. Figure 10 also shows the step by step procedure used in the design. To satisfy the conformality RFID requirements, the proposed antenna was fabricated on flexible 4-mil LCP. The IC used for this design has four ports; two input ports namely RF1 and RF2 are identical and may be connected to a single or dual antenna configuration. The resistive shorting stub and the

double inductive stub as illustrated in Figure 11 constitute the overall matching network. The resistive stub is used to tune the resistance of the antenna to match that of the IC. In this design the size and shape (thin long loop shaped line) of the resistive stub were designed to have an optimum match to Z_{IC}=73-j113 Ω. The double inductive stub is composed of two inductive stubs to provide symmetry on both sides of the antenna. The double inductive stub also serves as the reactive tuning element of the antenna.
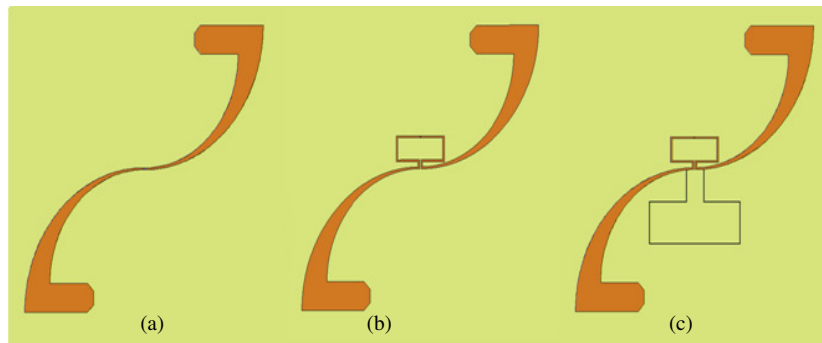
Figure 10. Step by step antenna design showing (a) Radiating body (b) Radiating body plus double inductive stub and (c) final antenna structure with the resistive stub.

The feeding point of the antenna is at the bottom part of the double inductive stub where an IC would be surface mounted. Figure 11 illustrates the final structure.

The stubs were designed to have a center frequency f_0 at 895 MHz with a bandwidth of 70MHz operating from 860→930 MHz (European and U.S. frequencies). A wide frequency sweep has also been performed up to 5 GHz where no parasitic radiation has been observed for this antenna. Those variables can be fine tuned to optimize the antenna characteristics on the RFID tag at any frequency and matched to any IC impedance.

16
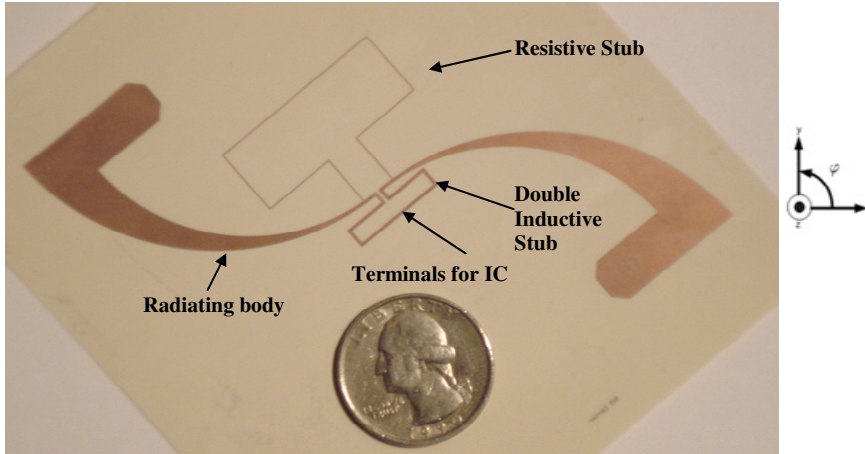
Figure 11. RFID antenna structure showing stubs.

The structure was simulated and optimized in the system level design tool HFSS. The input impedance of the simulated antenna design is shown in Figure 12. As it can be observed the RFID UHF band (860→930 MHz) is outside the antenna self-resonance peak, resulting in a more flat impedance response against frequency. This yields to a bandwidth of ~8% which is predominantly realized by the finite slope of the reactance of the antenna in the frequency of interest.
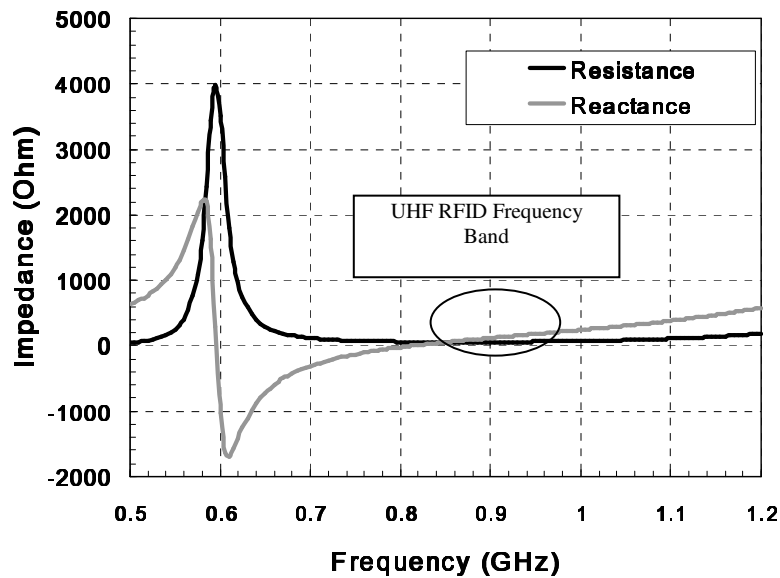
Figure 12. Simulated input impedance of the S-shaped antenna.

The simulated impedance at the center frequency f_0= 895 MHz is 57.46+j112.1 which results in a return loss RL<-18dB. This antenna has a bandwidth of ~8% (70 MHz) where the bandwidth is defined by a Voltage Standing Wave Ratio (VSWR) of 2 (alternatively a RL of -9.6 dB) as shown in the Results and Discussion section.

The return loss of this antenna was calculated based on the power reflection coefficient which takes into account the capacitance of the IC [23]:

$$\left| s^2 \right| = \left| \frac{Z_{IC} - Z_{ANT}{}^*}{Z_{IC} - Z_{ANT}} \right|^2 \tag{3}$$

Z_{IC} represents the impedance of the IC and Z_{ANT} represents the impedance of the antenna with $Z_{ANT}{}^*$ being its conjugate.

The simulated radiation pattern and radiation efficiency were numerically computed in HFSS by introducing an RLC boundary along with the port impedance that simulates the behavior of the IC (with its complex impedance feed). In Figure 13 the 2-D radiation plot is shown for the phi=0° and phi=90° (as defined in Figure 11) where an omnidirectional pattern is realized. The radiation pattern throughout the bandwidth of the antenna has also shown to have an omnidirectional pattern similar to that of a classic (λ/2) dipole antenna.

A directivity of 2.10 dBi is achieved with a radiation efficiency of 97%. The omnidirectional radiation is one of the most fundamental requirements for RFID's to allow for their reading/writing operation independent of the orientation of their antenna with respect to the reader.
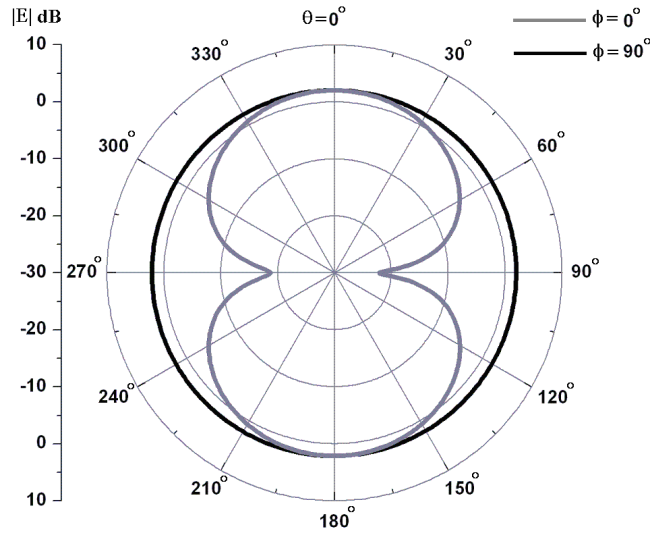
Figure 13. 2D far-field radiation plot for S-shape antenna.

4.2.2 Antenna Circuit Modeling

In order to obtain a thorough understanding of the power reflection caused by any mismatch at the terminals of the feed structure of the antenna, a wideband equivalent circuit model has been developed. This model serves as a benchmark for the design of an RFID antenna to theoretically match any Z_{IC} for maximum power flow resulting in optimum antenna efficiency and an excellent read range.

Based on a physical approach, an equivalent lumped element circuit model was derived. The system level design and simulation tool Advanced Design System (ADS) was used to simulate the behavior of the circuit model (S_{11} parameter) and resulted in a negligible error function ($<10^{-5}$). Figure 14 below shows the agreement between the lumped element circuit S parameters with that of the structure (from the full wave simulator).

19
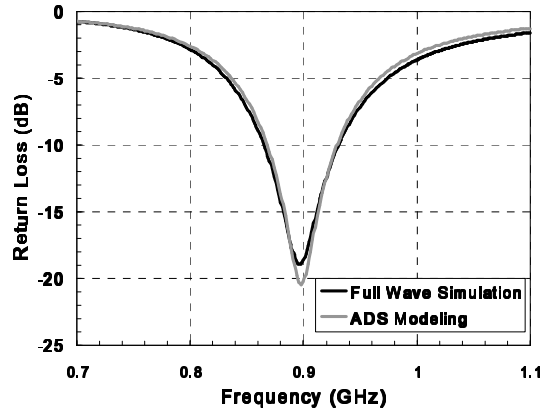
Figure 14. S_{11} for the exact structure and for the equivalent circuit model.

Figure 15 shows the detailed equivalent circuit of the radiating body only. Each arm of the radiating body consists of a resistor in series with an inductor, the combination of which models the metal effects. A capacitor in series with a resistor, which are located in parallel with the previous combination of L_s and R_s model the substrate effects. Finally, the capacitive coupling or E-Field coupling between the two arms of the S-shaped antenna is modeled by the top and bottom capacitors (for air and dielectric capacitive coupling respectively). This lumped element model covers a frequency range 700→1100 MHz as shown in Figure 14 above.
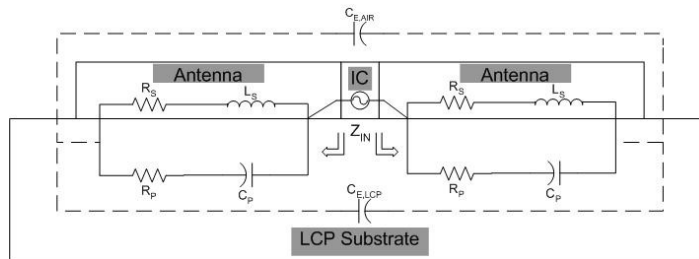
Figure 15. Cross-sectional detail showing equivalent lumped element model of RFID antenna shown in Figure 10 (a) and 10(b).

The circuit configuration in Figure 15 can be simplified to the one shown in Figure 16 by using symmetry and direct circuit analysis.

20
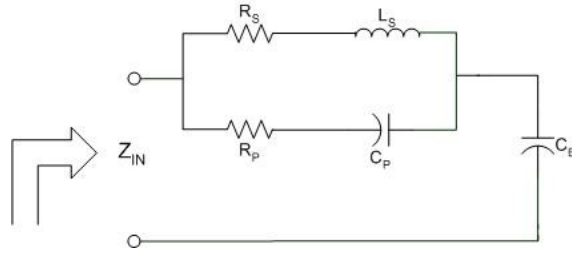
Figure 16. Equivalent circuit model of RFID antenna shown in Figure 10(a) and 10(b).

Since the double inductive stub is connected in series with the radiating body, the equivalent circuit model of the second stage design (radiating body plus inductive stub) as shown in Figure 10 has the same circuit elements configuration as the one in Figure 16, with change in values only. The final stage of the design has the circuit model configuration shown in Figure 17. Due to the configuration of the resistive shorting stub (connected in parallel with the radiating body plus inductive stub), the components: R_{s2}, L_{s2}, R_{p2}, C_{p2} are introduced as shown in Figure 17 below and model the same effects as those discussed previously for radiating body circuit model (Figure 16).
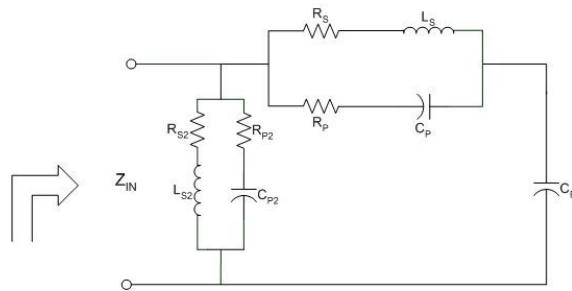
Figure 17. Equivalent circuit for antenna structure shown in Figure 10(c).

The equivalent circuit shows how stubs can be used to tune the impedance in order to match to any IC. Parametric sweeps can be used along different stubs structures (for example loops structures can be used for adding series inductance or parallel capacitance). The resistance of the antenna is mainly determined by the radiating body and can be tuned by the two stubs as shown above. This model also helps to determine the amount of loss (as parallel resistance and

21

capacitance) due to the substrate loss which helps in understanding radiation efficiency as a function of the substrate.

4.2.3 Measurement Results and Discussion

In order to accurately measure the input impedance of the RFID antennas, numerous problems should be taken into consideration. First of all, a traditional probe station was not suitable for our tests due to the undesired shorting effect of the metallic chuck, which was behaving as a spurious ground plane for the dipole antennas. To tackle the problem, a custom-made probe station using wood and high density polystyrene foam was built. This type of foam was selected due to its low ε_r of 1.06 [22] resembling that of the free space. A $5 \cdot \lambda/2$-thick foam station was designed in order to ensure minimum backside reflections of the antenna.

It was also taken into account the fact that the antennas were balanced structures and a typical GS probe connected to a regular coaxial cable would provide an unbalanced signal. To prevent a current difference between the dipole arms, a $\lambda/4$ balun with an operational bandwidth of 840$\rightarrow$930 MHz (which covers the band of interest for the design) was used. After all the above mentioned precautions were taken and minding about the calibration process, S-parameters were measured using Agilent 8510C VNA and transformed to Z_{IN} or Z_{ANT}.

Figures 19 and 20 show a very good agreement between the simulated results and the measurements for the antenna input impedance and S_{11} parameter respectively. The demonstrated antenna bandwidth allows for a universal operation of the proposed UHF RFID (Worldwide frequency coverage except Japan and some Asian countries that operate at a frequency of 950 MHz and higher) frequency band.
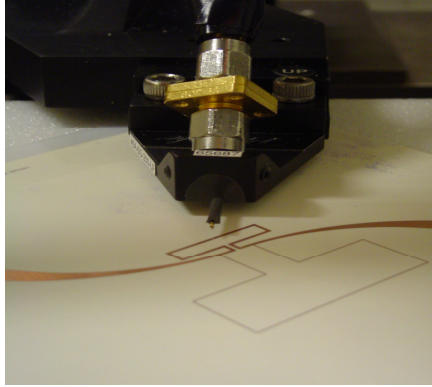
Figure18. Photograph of the probe plus S-shaped antenna.
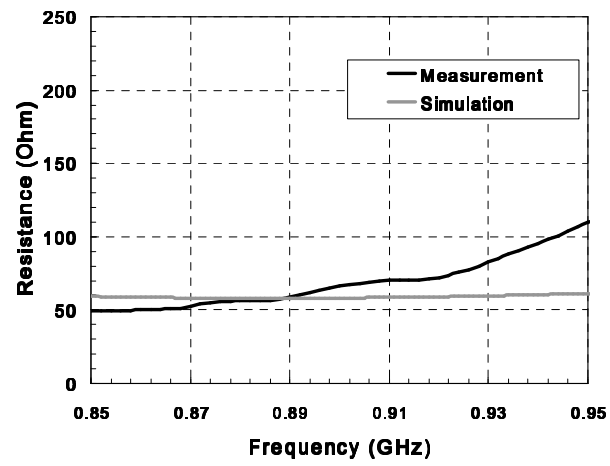
(a)
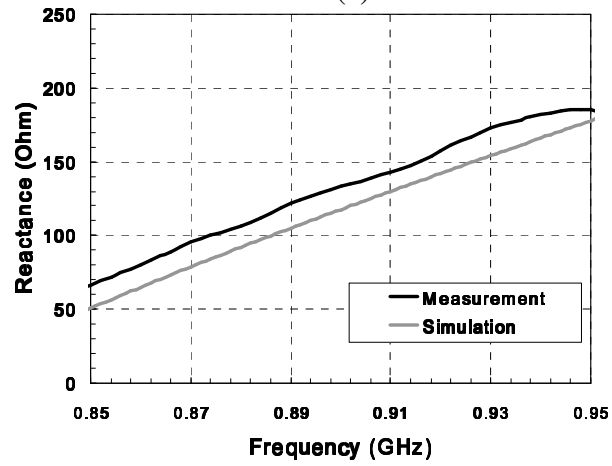
(b)

Figure 19. Measured and simulated data of input impedance: (a) Resistance (b) Reactance.
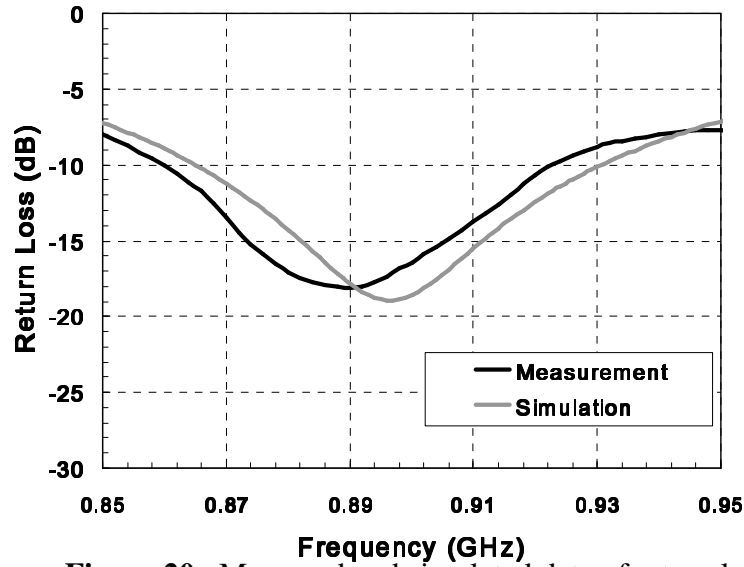
Figure 20. Measured and simulated data of return loss.

4.2.3 Effect on Antenna Parameters when placed on Common Packaging Materials

In order to fully investigate the effect of the surroundings on the antenna parameters, such as the resonance, bandwidth, and radiation; the S-shaped antenna was simulated for 3 practical configurations: on a 4mm thick common plastic material [PET-Polyethylene terephthalate (ε_r=2.25 and tanδ=0.001)], on 4mm thick paper (ε_r=3.28 and tanδ=0.006[8]) substrate as well in an embedded structure with 0.5mm thick paper superstrate on a 4mm paper substrate. Figure 21 shows the Return Loss results for the polyethylene and paper substrates. A shift in resonance frequency occurs (95 MHz for paper and 60 MHz for PET from the original antenna with center frequency 895MHz on LCP substrate). This observation can be easily corrected by scaling down the x-y dimensions of the antenna. In the paper case the antenna was scaled down by 13% while the antenna on PET by a factor of 8% and the new Return Loss results as shown in Figure 22 were obtained. As seen in the figure, the detuning of the resonance can be easily performed by scaling the whole structure. For example, when placed on paper substrate, detuning becomes necessary if the thickness exceeds 1.5mm.

24

As for the most common case where these RFID tags are placed on cardboard boxes; the dielectric properties of cardboard do not impede antenna characteristics due to its low dielectric constant (close to 1 and low loss properties [30]). However, the effect of the enclosed materials and the distance of the RFID tag from the arbitrarily placed enclosed contents play a more important role than the size and thickness of the cardboard. An alternative way to increase the bandwidth of the antenna in order to compensate for the material/fabrication variations is the use of a more broadband matching section, potentially introducing an additional stub-line.
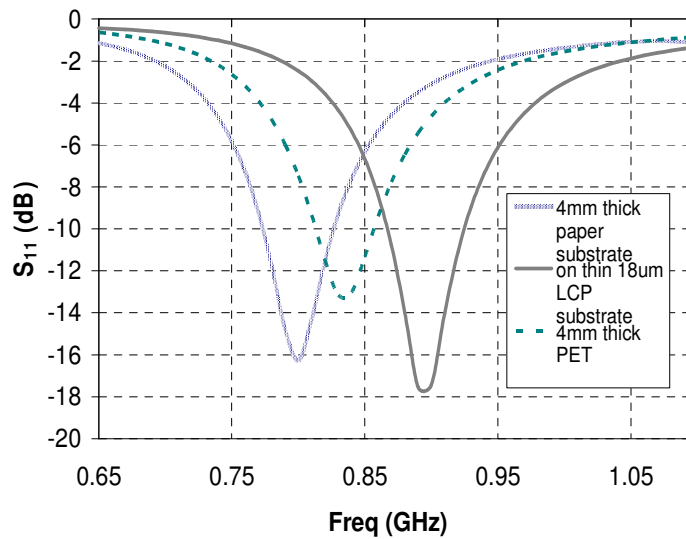
Figure 21. Return loss for 4mm thick paper and PET substrates.
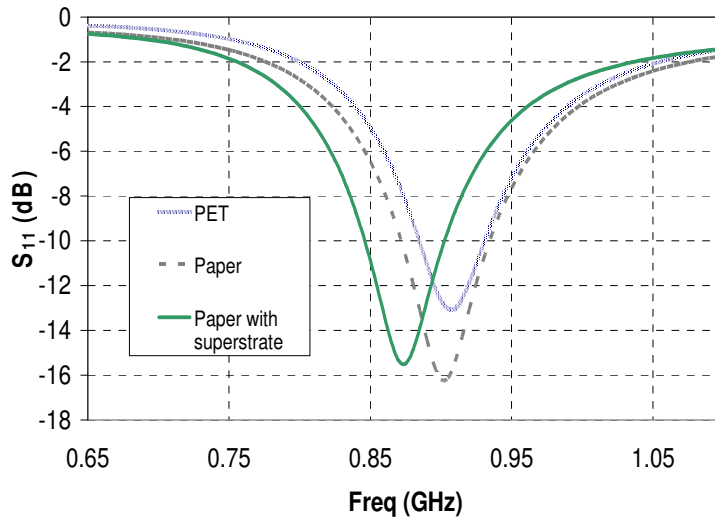
Figure 22. Return loss for 4mm thick paper and PET substrates with modified Antenna Dimensions.

25

In order to analyze the effect of the radiation pattern of these materials, the gain for the S-shaped antenna has been plotted in Figure 23 for the LCP and paper substrates. The worst case scenario observed for gain loss was 1.049 dB (on 4mm paper) for the E-plane or φ=0 degrees plane in comparison with 2.095 dB (on 18 um LCP).
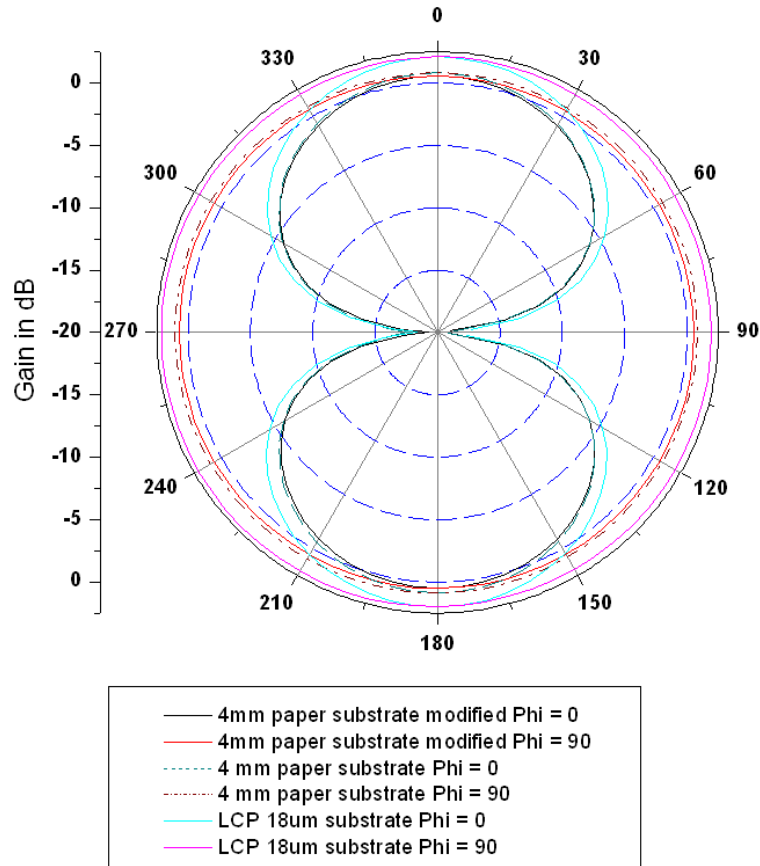
Figure 23. Radiation Pattern of the Gain of the s-shaped antenna on paper, and LCP substrates.

4.3 Bowtie T-match RFID Antenna

4.3.1 Design Approach

In this section a T-match folded bow-tie half-wavelength dipole antenna [20] was designed and fabricated on a commercial photo paper by the inkjet-printer mentioned above. The antenna was designed using Ansoft's HFSS 3-D EM solver. This design was used for the matching of the passive antenna terminals to the TI RI-UHF-Strap-08 IC with resistance R_{IC} = 380 Ohms and reactance modeled by a capacitor with value C_{IC}=2.8 pF [22]. The IC was modeled in HFSS by introducing a lumped port and an RLC boundary. The lumped port was specified to be a purely resistive source with R=380 Ohms and the RLC boundary was specified to have a Capacitance value of 2.8 pF; hence simulating the IC's complex impedance. The RFID prototype structure is shown in Figure 24 along with dimensions, with the IC placed in the center of the T-match arms. The T-match arms are also responsible for the matching of the impedance of the antenna terminals to that of the IC through the fine tuning of the length L3, height h, and width W3. The current distribution of this antenna at 900MHz is shown in Figure 25.
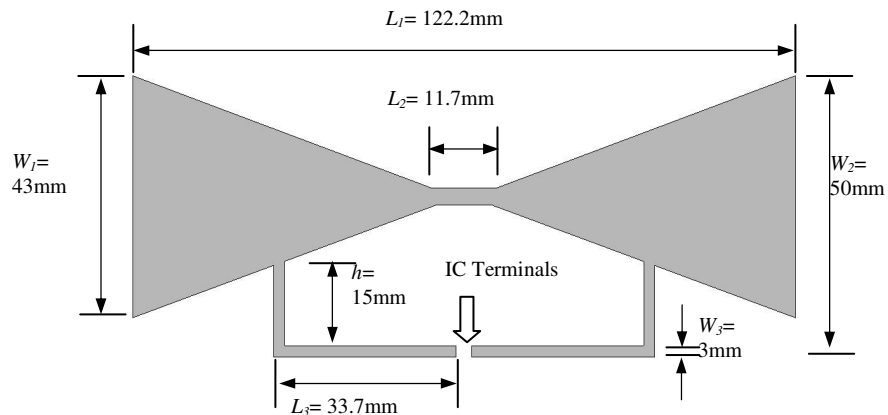
Figure 24. T-match folded bow-tie RFID tag module configuration.

4.3.2 Results and Discussion

A GS 1000μm pitch probe connected to a UHF balun to ensure the balanced signal between the arms of the T-match folded dipole antenna was used for impedance measurements, as shown in Figure 26. In order to minimize backside reflections of this type of antenna, the fabricated or inkjet printed antennas were placed on a custom-made probe station as discussed insection 4.2.3. The calibration method used was short-open-load-thru (SOLT). Figure 27 shows the impedance plots. As shown in Figure 27(a), the simulated resistance for the antenna in the UHF RFID frequency range maintains a value close to 380 Ohms between the two successive peaks. The reactance part of the impedance, as shown in figure 27(b), features a positive value with a linear variation with frequency, pertaining to an inductance that conjugately matches or equivalently cancels the effect of the 2.8pF capacitance of the IC. Fairly good agreement was found between the simulation and measurement results. The distortion is possibly due to the effect of the metal probe fixture.

The return loss of this antenna was calculated based on the power reflection coefficient as shown in equation 3 in section 4.2.1. The plot is shown in figure 28 demonstrating a good agreement for both paper metallization approaches. The nature of the bow-tie shape of the half-wavelength dipole antenna body allows for a broadband operation, with a designed bandwidth of 190MHz corresponding to 22% around the center frequency 854 MHz which covers the universal UHF RFID bands. It has to be noted that the impedance value of the IC stated above was provided only for the UHF RFID frequency which extends from 850MHz to 960MHz; thus, the return loss outside this frequency region, shown in Figure 28, may vary significantly due to potential IC impedance variations with frequency.

In order to verify the performance of the ink-jet printed RFID antenna, measurements were performed on a copper-metalized antenna prototype with the same dimensions fabricated on the same paper substrate using the slow etching technique mentioned before. The return loss results are included in Figure 28 and they show that the return loss of the inkjet-printed antenna is very slightly larger than the copper one. Overall a good agreement between the copper etched and the inkjet-printed antennas was observed despite the higher metal loss of the silver-based conductive ink.

The radiation pattern was measured using Satimo's Stargate 64 Antenna Chamber measurement system as shown in Figure 29 and by using the NIST Calibrated SH8000 Horn Antenna as a calibration kit for the measured radiation pattern at 915 MHz. The radiation pattern as shown in Figure 30 is almost uniform (omnidirectional) at 915 MHz with directivity around 2.1dBi. The IC strap was attached to the IC terminal with H2OE Epo-Tek silver conductive epoxy cured at 80°C. An UHF RFID reader was used to detect the reading distance at different directions to the tag. These measured distances are theoretically proportional to the actual radiation pattern. The normalized radiation patterns of simulation, microwave chamber measurement and reader measurement are plotted in Figure 30, showing a very good agreement between simulations and measurements, which can be also verified for other frequencies within the antenna bandwidth.
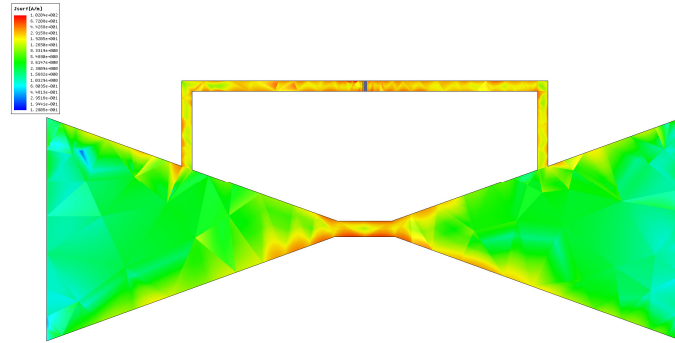
Figure 25. Simulation plot of current distribution at 900MHz.
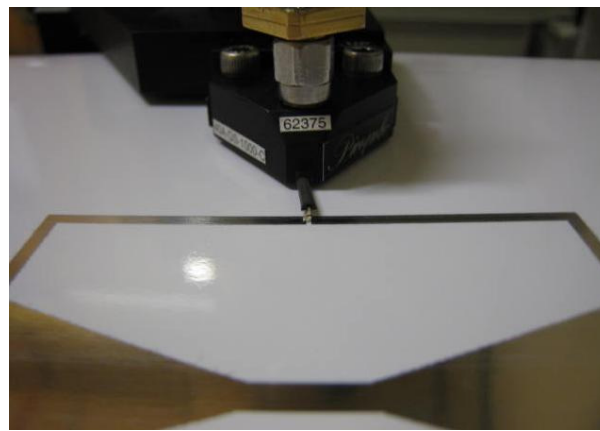
Figure 26. Photograph of the impedance measurement using GS pitch probe.
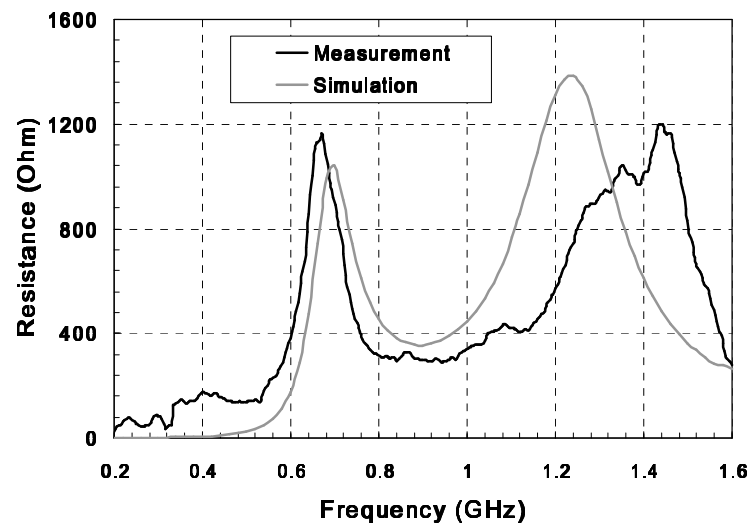
(a)
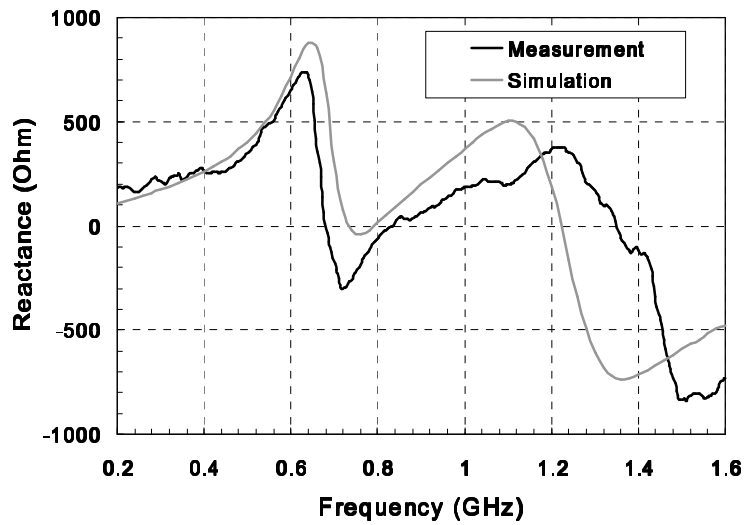
(b)

Figure 27. Measured and simulated input resistance and reactance of the inkjet-printed RFID tag, (a) Resistance (b) Reactance.
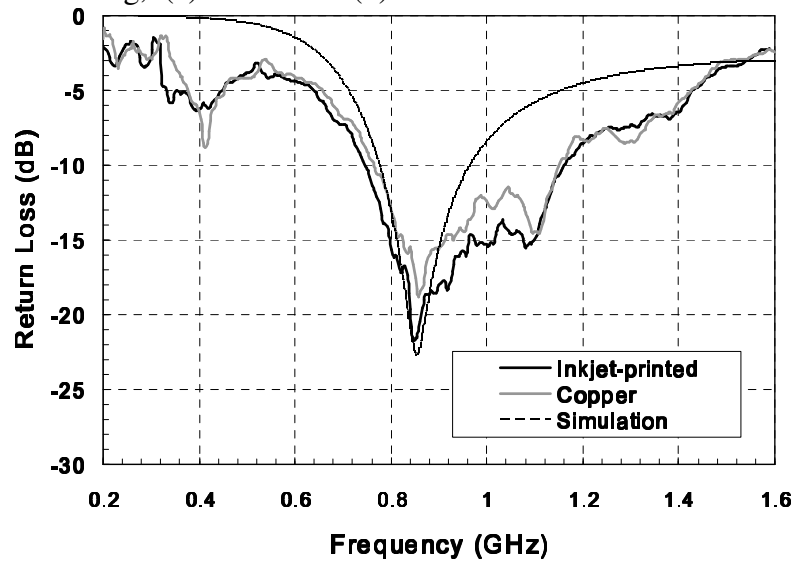
Figure 28. Measured and simulated Return Loss of the inkjet-printed RFID tag
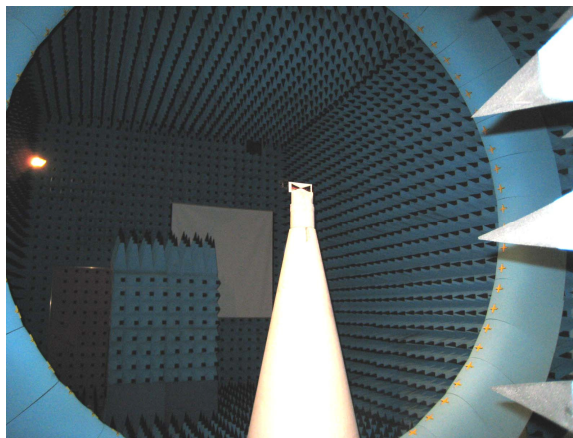
Figure 29. Photograph of the radiation pattern measurement in an Antenna Chamber.

31
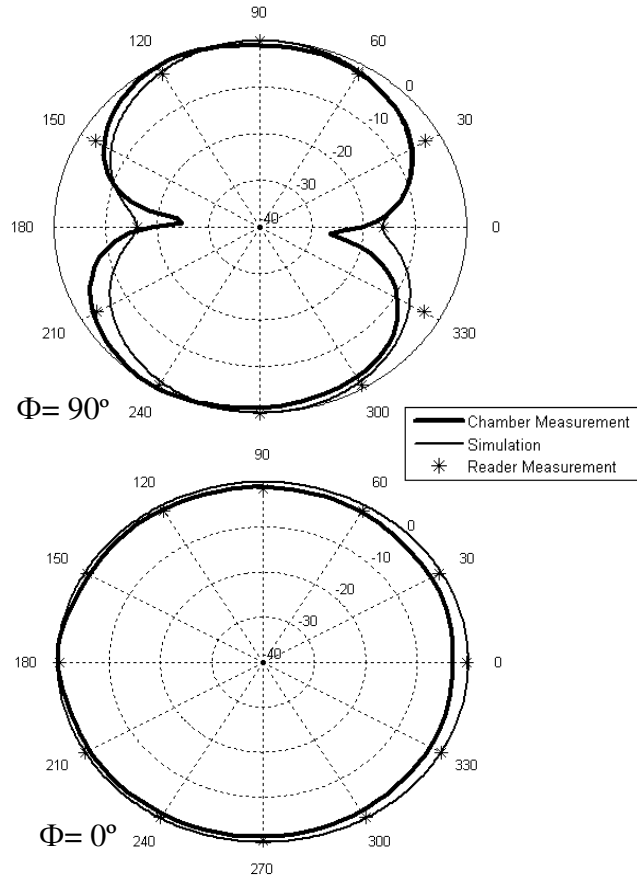
Figure 30. Normalized 2D far-field radiation plots of simulation, chamber measurement and tag reading distance measurement.

4.4 Monopole Antenna

Minor drawbacks that might occur with the dipole based module can be eliminated by using a monopole based structure. Unlike the dipole antenna which has no ground, the monopole uses its ground planes as a radiating surface, which can also be used to shield any circuitry behind it. The monopole antenna also does not require a differentially fed input signal like the dipole, which is ideal for Power Amplifiers (PA) since their output might be single-ended. This section gives guidelines on designing a monopole antenna that can be used for Identification and Sensing applications.

4.4.1 Design Approach

The geometry and a photograph of the proposed CPW-fed printed monopole antenna is shown in Figure 31. This module uses paper as a substrate, with a thickness of 0.254mm, and overall dimensions 75mm (width) x 100mm (length), including the feeding line. A Coplanar Waveguide (CPW) transmission line consisting of a single metallic layer is selected for feeding the antenna because of its easy integration on the paper substrate due to its planar structure. The antenna structure is composed of a planar Z-shaped rectangular monopole with width 50mm, length 56mm and a spacing of h=11mm from the ground plane. Two rectangular slots are embedded into the radiating element from both side edges, resulting in a meander-like antenna as shown in Figure 31. Both slots have a width of 10mm and lengths of l1=l2=40mm, chosen to optimize the matching of the antenna to the load.
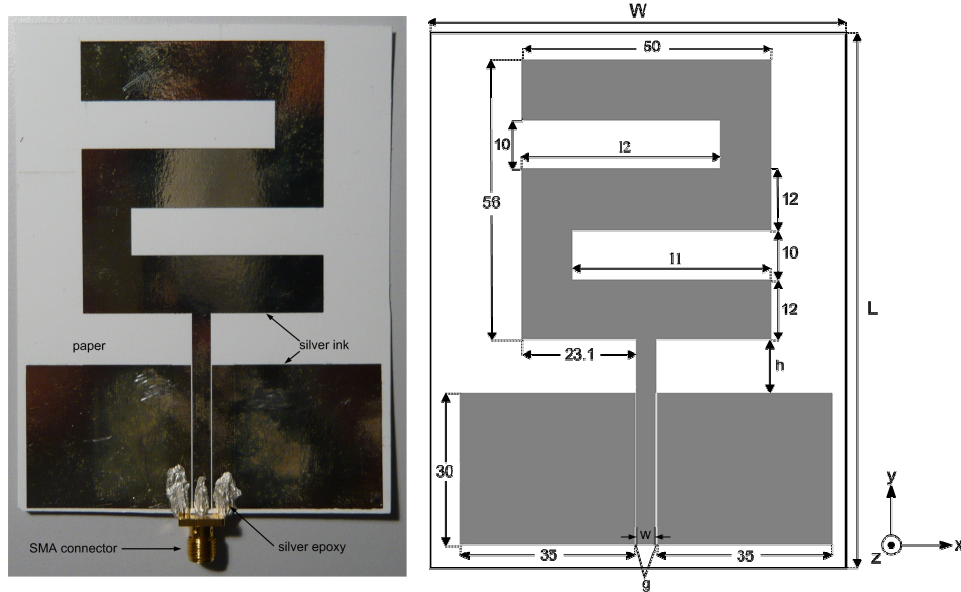
Figure 31. Photograph and Schematic (units in mm) of the proposed monopole antenna.

As discussed earlier, RFID antenna design should fulfill several design requirements: "global-operability" UHF bandwidth [USA (902–928 MHz), Europe (865–868 MHz)] RFID band, omnidirectional radiation pattern, impedance matching with RFID circuitry, long read range, and compact size. Optimizing these parameters involves however inevitable tradeoffs between them [19]. Maximizing the size of the ground plane increases the directivity of the antenna, because the ground acts as a radiating element and also shields it from the rest of electronic circuitry; however it increases the profile of the antenna. Impedance matching in RFID tags between the antenna and the load is very significant for the range maximization. In order to ensure maximum power transfer from the antenna to the load, the antenna was matched to an impedance of 60.1-j73.51 ohms ($Z_{L\text{-opt}}$) which is the reference at the PA output (to be integrated with this antenna module) at the design frequency of 904.4 MHz. The parameters h, g, and w were also optimized to fine tune the desired antenna impedance and increase the directivity. The height (h) of the radiating element from the ground has a major influence on the performance of

the antenna, as it modifies the radiation pattern and the impedance of the antenna. By increasing it, guided waves of the antenna are transitioning more efficiently into free-space waves and the impedance becomes more capacitive. Maximizing it however results into thick and difficult to mount RFID tags. The value of the parameters after optimization where found h=11mm, g=0.3mm and w=3.8mm.

4.4.2 Results and Discussion

The performance of two prototypes (inkjet-printed and copper tape fabricated) was experimentally tested and the results are presented in Figure 32, which shows the simulated and measured Return Loss featuring a good agreement. It can be seen from the simulations that the inkjet-printed antenna has a resonance at 904 MHz and a –10dB impedance bandwidth of 132 MHz (822–954MHz) corresponding to 14.6% around the resonant frequency. The measured S_{11} plot of the inkjet-printed antenna is resonant at 898Mhz with bandwidth of 82Mhz (860–942MHz) corresponding to 9.1% around the resonant frequency, where the copper tape fabricated antenna displays a return loss plot with resonant frequency at 906Mhz and a bandwidth of 68Mhz (874 – 942MHz) corresponding to 7.5%. The radiation characteristics of the proposed antenna have also been investigated and are depicted in Figure 33. The simulated radiation patterns for the x-z plane and the y-z plane at the resonant frequency 904.5 MHz demonstrate a radiation pattern similar to a conventional monopole antenna, displaying an omnidirectional radiation pattern on the x-z plane and a directional pattern with 2 nulls on the y-z plane. The directivity of the antenna was found 0.2dBi in simulation.
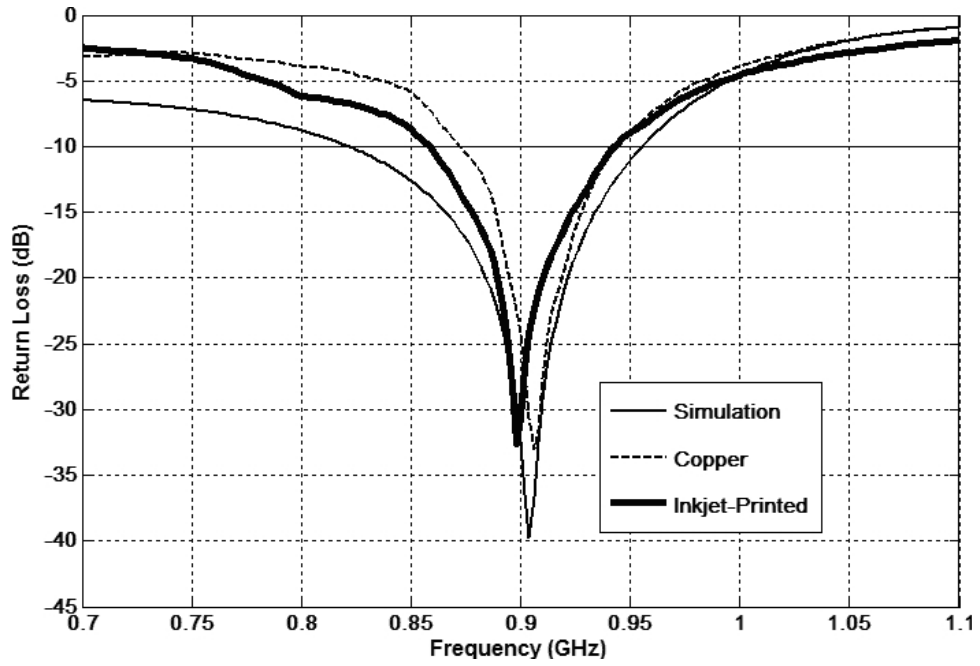
Figure 32. RL of the inkjet printed and copper tape fabricated monopole antenna.
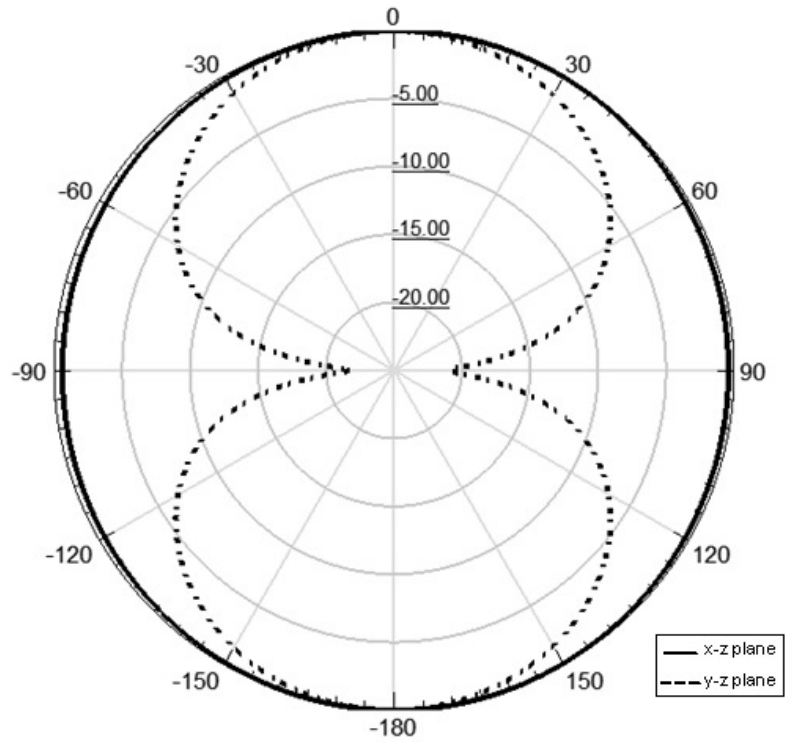
Figure 33. Simulated radiation pattern of monopole antenna at 904.5 MHz.

4.4.3 Antenna Gain Measurement

The following equipment was used to carry out the gain measurements for the inkjet-printed and copper fabricated UHF monopole antenna:

- ROHDE & SCHWARZ SMJ 100A Vector Signal Generator

- Tektronix RSA3408A DC – 8GHz Real Time Spectrum Analyzer

- AN-400 Reader Antenna with gain G_r=6dBi

- Typical 3.5mm Coaxial Cable with attenuation=0.1dB

The equipment was set up as shown in Figure 34. The prototype antenna to be measured was treated as the transmitter and was connected with a coaxial cable to the Vector Signal Generator. The antenna (transmitter) was attached at a height of h_t=1.60m on a piece of polystyrene foam using thin adhesive tape, as shown in Figure 35. Polystyrene foam was used to hold the antenna in place, simulating a free-space environment. The AN-400 antenna is a commercial RFID reader antenna and is treated as the receiver in the experimental setup The receiver was connected with a coaxial cable to the Real Time Spectrum Analyzer and was positioned at a fixed place that had also a height of h_r=1.60m, as shown in Figure 36. Both distances were measured from the middle point of each antenna to the ground. The distance between the transmitter and the receiver was measured d=4.06m.
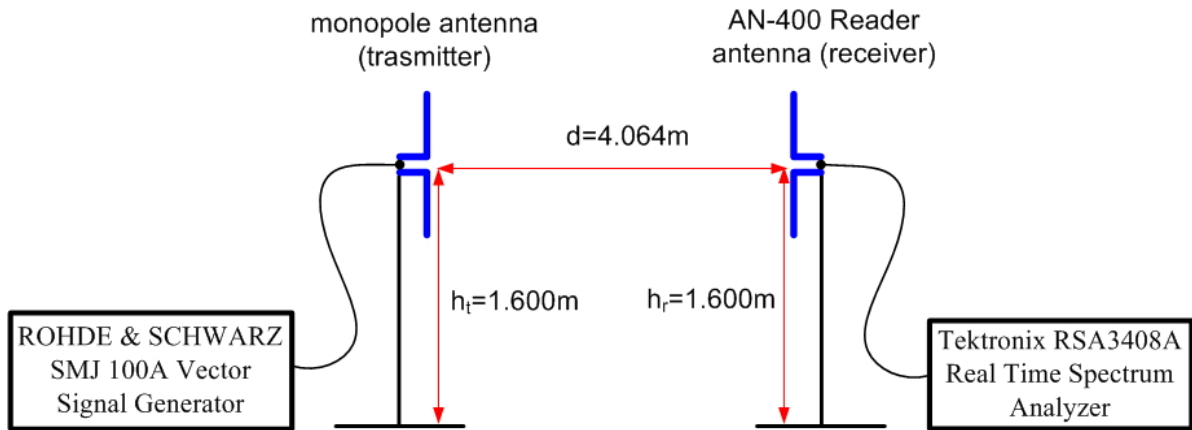
Figure 34. Gain measurement experimental setup
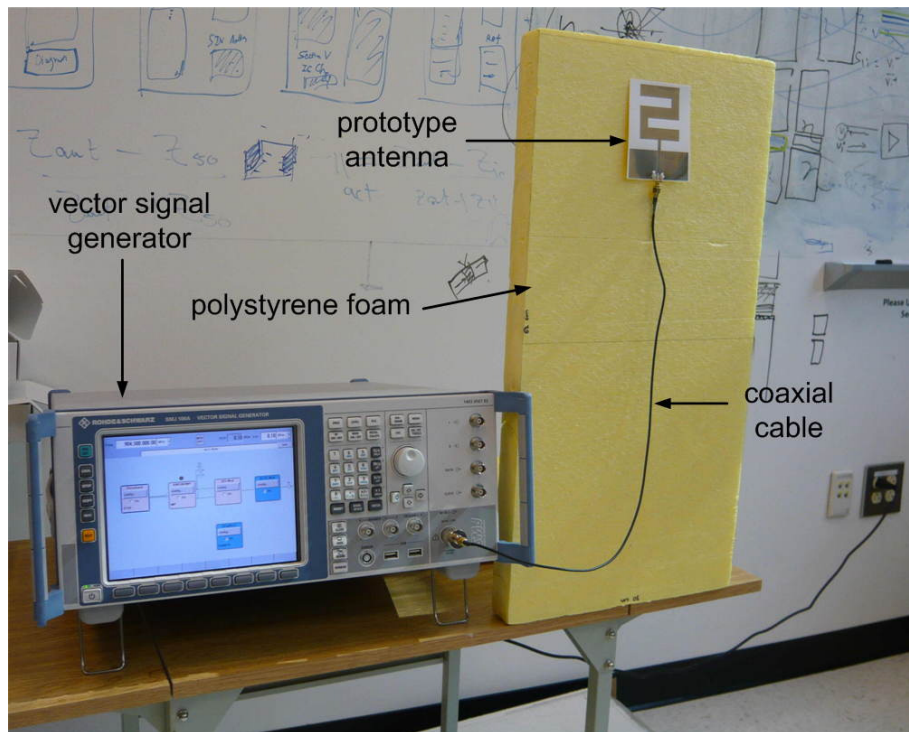
Figure 35. Prototype antenna (transmitter) and vector signal generator setup.
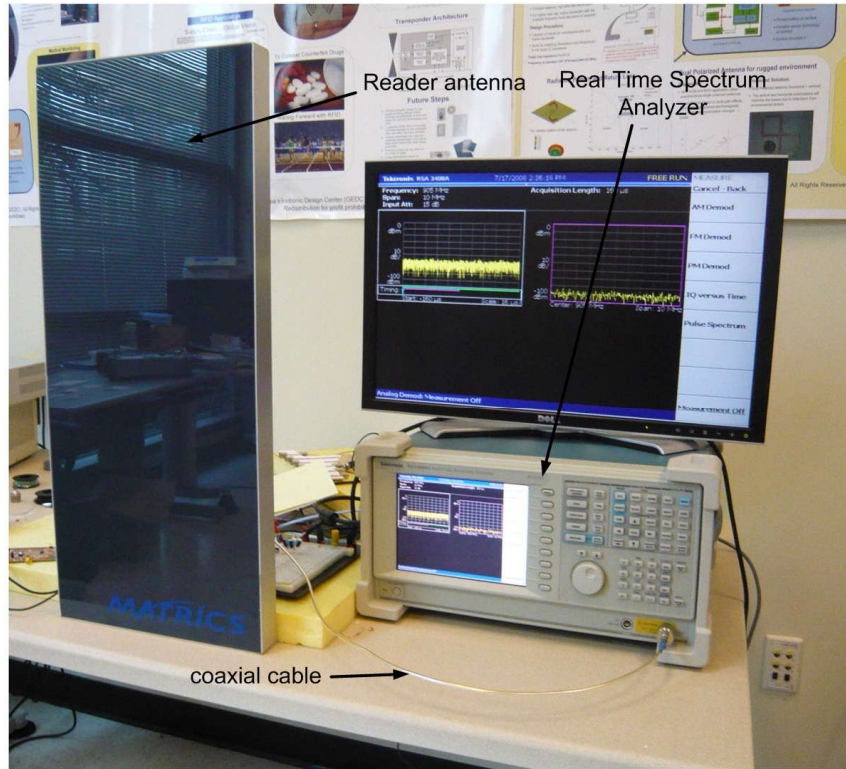
Figure 36. AN-400 RFID reader antenna (receiver) and real time spectrum analyzer setup

Verifying that the receiver is at the far field region of the transmitter was performed as a

first step using Fraunhofer's far field equation, shown below:

$$R = \frac{2D^2}{\lambda}$$
(4)

where:

R: the distance from the prototype antenna at which its far field region starts

D: the largest dimension of the antenna

λ : the free space wavelength at the transmission frequency of 904.5MHz

The far field boundary for the monopole antenna is evaluated using (4) to be *R=6.0cm*

Therefore it is verified that the receiver is in the far field region of the monopole antenna. It is

also essential to make sure that there is a clear line of sight between the two antennas and that no

other objects are at a smaller distance from the antenna's far field boundary d_t. Finally it is

critical that both antennas are placed in the optimum orientation with each other. Each antenna must be placed in the direction of maximum radiation intensity or gain of the other. In this way the gain of the fabricated antenna can be measured correctly at the operating frequency and compared to the simulation. The gain measurement is performed for both the inkjet-printed and the copper fabricated antenna. The Vector Signal Generator is set so that it transmits a continuous wave signal at the operating frequency of the antenna, which is at 904.5MHz with power $P_s=0.1dBm$. The Signal Generator is connected to the antenna, with a 50Ω coaxial cable with loss $L_c=0.1dB$. Therefore, the power at the end of the coaxial cable and before the input of the antenna is $P_t = P_s - L_c = 0dBm$.

In addition the antenna is not matched to the 50Ω coaxial cable, since it has complex input impedance. As a result there is another power loss in the antenna input because of power reflection, between the antenna and the 50Ω transmission line. The reflection coefficient ρ for the both inkjet printed and copper fabricated antenna is calculated by (5) taking into account their respective measured input impedance at the operating frequency.

$$\rho = \frac{Z_{ant} - Z_0}{Z_{ant} + Z_0} \tag{5}$$

where:

Z_{ant} : the measured input impedance of the antenna at the operating frequency

Z_0 : the characteristic impedance of the coaxial cable (Z_0=50Ω)

ρ : reflection coefficient

The magnitude of ρ is found for the inkjet printed antenna $|\rho| = 0.59$ and for the copper

tape fabricated antenna $|\rho| = 0.60$. The mismatch loss is evaluated for both antennas as:

$$L_m = \left(1 - |\rho|^2\right)_{dB} = 1.9\text{dB}.$$

The input power after the losses is radiated from the proposed antenna (transmitter) into

space and is received by the Reader Antenna (receiver). The reader antenna has gain of G_r=6dBi

and is matched to the 50Ω coaxial cable that connects it to the spectrum analyzer. Because the

receiver antenna is circular polarized and the transmitter monopole antenna is linear polarized, a

polarization mismatch exists in the wireless link between the two antennas. The polarization

mismatch has to be accounted and is assumed to be L_p=3dB. The accepted power from the reader

antenna is measured by the spectrum analyzer, which was set to a center frequency of 904.5MHz

with a resolution bandwidth of 36MHz. The measured accepted power results are the same for

both antennas and are illustrated in Figure 37.
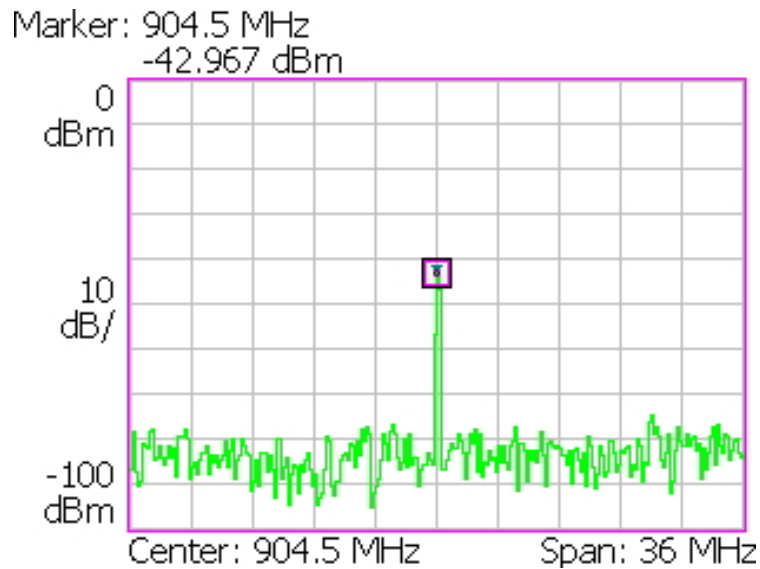
Figure 37. Received power at the AN-400 RFID reader antenna (receiver) terminals

In order to calculate the gain of the antenna from the measured results, a propagation model has to be applied. To determine which propagation model is suitable for our measurement setup, an investigation to whether any obstacles exist in the first Fresnel zone of our wireless link setup was performed. Therefore, the maximum radius of the first Fresnel zone has to be calculated. The maximum radius of the first Fresnel zone is calculated by determining the radius of the Fresnel zone cross section from (6) at the midpoint between the transmitter and the receiver, as shown in Figure 38.

$$r = \sqrt{\frac{\lambda}{\left(\frac{1}{d_t} + \frac{1}{d_r}\right)}} \tag{6}$$

where:

r : the radius of the first Fresnel zone

λ : the wavelength of the transmitted signal in free space

dt : the distance from the fresnel zone cross section to the transmitter

dr : the distance from the fresnel zone cross section to the receiver

The radius r, when $d_t = d_r = 2.03$m is found r=0.58m. It is observed that r is lower than the heights of the transmitter and the receiver and since no object exists between them, the requirement of clearance of the first Fresnel zone is satisfied. As a result the free space loss model can be applied as the propagation model in the wireless link of the two antennas.
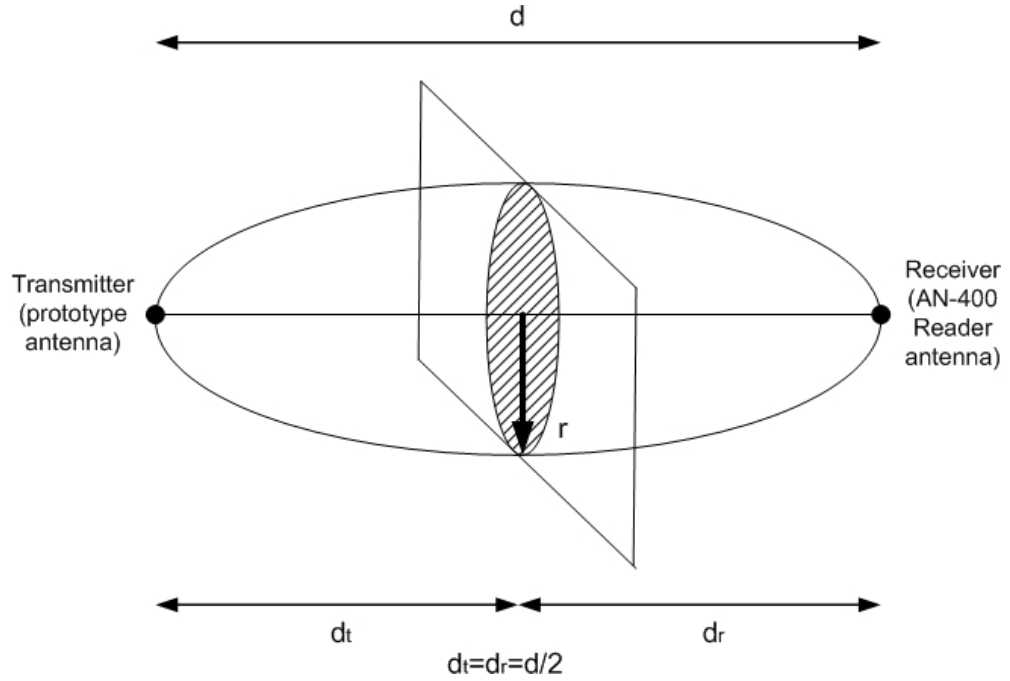
Figure 38. First Fresnel zone cross section at the middle point of the wireless link setup between the prototype antenna and the reader antenna (receiver)

Since the free space loss propagation model can be applied, the gain of each prototype antenna will be calculated using the Friis transmission equation [19]. The power received by an antenna is described by the Friis formula, which accounts for all antenna gains, path loss and losses in the system and is given for the current measurement by (7)

$$\frac{P_r}{P_t} = G_t G_r \left(1 - |\rho|^2\right) |\hat{\rho}_t \cdot \hat{\rho}_r|^2 \left(\frac{\lambda}{4\pi d}\right)^2 \tag{7}$$

where

P_t : the radiated power from the transmitter antenna

P_r : the received power from the receiver antenna

ρ : the complex reflection coefficient at the input of the transmit antenna

$\hat{\rho}_t$: polarization unit vector of the transmitter antenna

$\hat{\rho}_r$: polarization unit vector of the receiver antenna

43

The Friis formula can be written in a decibel form, as shown in the equation below:

$$P_r = P_t + G_t + G_r - L_m - L_p - 20\log_{10}\left(\frac{4\pi}{\lambda}\right) - 20\log_{10}(d) \qquad (8)$$

It has to be noted that the polarization mismatch is given by $|\hat{\rho}_t \cdot \hat{\rho}_r|^2$ and equals the mismatch loss L_m in dB. From the above equation the gain for both the inkjet printed and the copper tape antenna is calculated: $G_t = -0.33\text{dBi}$.

The obtained results, along with the results from the simulation are summarized in Table 2. In addition the design goals are also given for comparison: It has to be noted that the input impedance, directivity, gain, antenna efficiency and return loss are calculated at the required antenna operation frequency, at 904.5MHz. Since no radiation pattern measurements were carried out, the directivity and the efficiency of the monopole antenna could not be experimentally measured.

Table 2 Comparison of simulated and experimental results
of the proposed antenna with the design requirements

Antenna Parameter	Requirement	Simulation	Inkjet-Printed	Copper Fabricated
Center Frequency (MHz)	904.5	904	898	906
Operation Bandwidth (MHz)	≥866 – 928	822 – 954	860 – 942	874 – 942
Bandwidth (MHz)	≥62	132	82	68
Bandwidth (%)	≥6.9	14.6	9.1	7.5
Input Impedance (Ω)	≈37.3–j65.96	37.5–j65.2	36.2 – j61.5	39.5 – j65.4
Directivity (dBi)	≥0	0.23	-	-
Gain (dBi)	≥-1	-0.42	-0.33	-0.33
Efficiency	≥80	88.7	-	-
Return Loss (dB)	≥-15	–38.4	-23.7	-31.9

It is observed that the return loss and gain measured results are in close agreement with the simulation and therefore the antenna design requirements defined in the first step of the design process are satisfied. It is seen from the measured –10dB impedance bandwidth, that both the inkjet-printed and the copper tape fabricated antenna can operate efficiently across the USA

(902 – 928MHz) UHF RFID frequency band. The inkjet printed antenna can operate also in the Europe (866 – 868MHz) UHF RFID band, satisfying the design requirements.

As a result the feasibility of modeling, designing and efficiently printing antennas on paper substrate is verified. Paper proved to be an excellent candidate as an antenna dielectric substrate material, since its dielectric loss doesn't decrease significantly the antenna gain, as seen from the gain measurements results. The agreement of the inkjet printed antenna measured results with the simulation, qualifies the inkjet printing process as an efficient method for printing RF structures, such as antennas on paper substrate.

4.5. RFID/Sensor Integration

In addition to the basic RFID automatic Identification capabilities along with the technologies and designs discussed above, the capabilities of inkjet-printing technology in integrated wireless sensors on paper bridging RFID and sensing technology [31] is demonstrated. The aim is to create a system that is capable of not only tracking, but also monitoring. With this real-time cognition, the status of a certain object will be made possible by a simple function of a sensor integrated in the RFID tag. The ultimate goal is to create a secured "intelligent network of RFID-enabled sensors." This section shows a sensor-enabled RFID on-paper that uses Gen2 protocols as means of communication on paper substrate.

A microcontroller enabled wireless sensor module was realized on a paper-based substrate. The system level design for this wireless transmitter can be seen in Figure 39 below. At the heart of the unit was an integrated 8-bit microcontroller unit that was programmed to sample an analog temperature sensor, perform an analog to digital conversion of the sensed data, bit encode the digital form of the sensed data into full 2 sub carrier cycle Miller bits [3] and finally modulate the power amplifier in the integrated transmitter module in the same sequence

45

as bit encoded, digital sensor data using Amplitude Shift Keying (ASK) modulation. The transmission frequency of 904.4 MHz was generated by using a crystal oscillator that was connected to the input of the phase lock loop (PLL) unit of the transmitter. The data transmission was to be carried out at the unlicensed UHF frequency around 900 MHz.
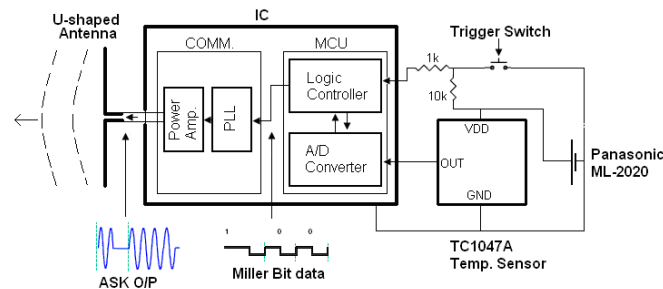

Figure 39. System level diagram of wireless sensor module.

The overall dimensions of the structure are: 9.5 x 5 cm and is shown in Figure 40.The antenna and traces are used for the assembling of the components: TC1047 Temperature sensor, TSSOP packaged IC, Inductors, Capacitors, Resistors, Crystal oscillator and Battery. The Return Loss or S_{11} recordings for the center frequency for the antenna terminals were recorded to be -15.05 dB for the simulated structure using the full wave EM simulator HFSS and -12.45 dB measured using the ZVA-8 VNA.The normalized radiation pattern as shown in Figure 41, was measured using Satimo's Stargate 64 Antenna Chamber measurement system and by using the NIST Calibrated SH8000 Horn Antenna as a calibration kit for the measured radiation pattern at 904 MHz. This prototype was tested for wireless transmission using a XR-400 RFID reader antenna interfaced to a Tektronix RSA 3408A Real Time Spectrum Analyzer (RTSA) and the measured power was recorded to be -68 dBm.

This module is easy to be extended to a 3D multilayer paper-on-paper RFID/Sensor module by laminating a number of photo-paper sheets (260um thickness/sheet). This is expected to drop the cost of the sensor nodes significantly and eventually made the "ubiquitous computing

network" a possible reality with a convergent ability to communicate, sense, and even process

information.
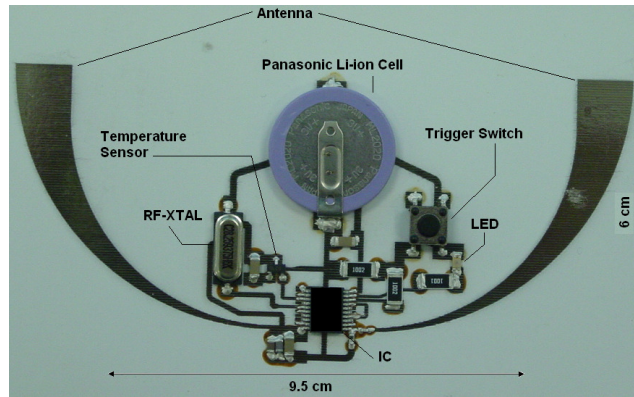
Figure 40. Wireless Sensor transmitter prototype on paper substrate using silver inkjet printing technology.
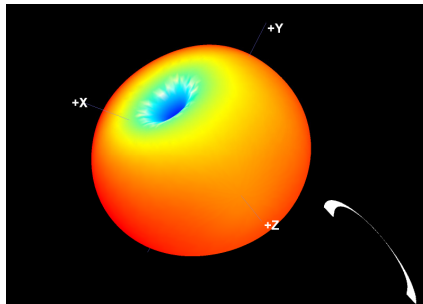
Figure 41. Measured normalized radiation pattern of U-shaped antenna.

CHAPTER 5

CONCLUSION

Paper which holds one of the biggest market share in the world can potentially revolutionize the electronics market and eventually take the first step in creating an environmentally friendly first generation of truly "green" RF electronics and modules. Not to mention that paper is one of the lowest cost materials produced. The inkjet printing technology, which is a much faster and cleaner method than the conventional wet etching techniques, which uses several "etchant" chemicals, can serve as low-cost mass-deployment technology for fabricating RFID tags to be produced in large reel to reel processes on paper. It can be easily verified that direct-write technologies such as inkjet printing, which consists of depositing nano-silver-particles, can be a very critical technology for the quick developing of next-generation flexible "cognitive" electronics due to its speed and ease of prototyping process. Three antenna modules have been presented. An S-shape dipole antenna using matching stubs that could potentially match the antenna for a wide range on IC impedances has been presented. A "Global" UHF passive RFID antenna using the classic T-match approach has been presented as the benchmarking prototype for this novel technology featuring an excellent performance for a wide ("universal") frequency range. A monopole Z-shaped antenna has been presented as a potential candidate for sensor integration. Last but not least, this work reported a 2D integrated-sensor with UHF RFID capabilities completely on paper, which could potentially set the foundation for the truly convergent wireless sensor ad-hoc networks of the future.

REFERENCES

[1]   K. Finkenzeller, RFID Handbook, 2nd ed., Wiley, 2004.

[2]   S. Basat, S. Bhattacharya, A. Rida, S. Johnston, L. Yang, M.M. Tentzeris, and J. Laskar, "Fabrication and Assembly of a Novel High-Efficience UHF RFID Tag on Flexible LCP Substrate," Proc. of the 56th IEEE-ECTC Symposium, pp.1352-1355, May 2006.

[3]   "UHF Gen-2 System Overview". Texas Instruments, Sept 2005, available HTTP: http://rfidusa.com/superstore/pdf/UHF_System_Overview.pdf

[4]   M. Lessard, L. Nifterik, M. Masse, J. Penneau, R. Grob, R, "Thermal aging study of insulating papers used in power transformers," Electrical Insulation and Dielectric Phenomena 1996, IEEE Annual Report of the Conference on, Volume 2, pp. 854 – 859, 1996.

[5]   L. Yang, A. Rida, R. Vyas, M. M. Tentzeris, "RFID Tag and RF Structures on a Paper Substrate Using Inkjet-Printing Technology," Microwave Theory and Techniques, IEEE Transactions on Volume 55, Issue 12, Part 2, Dec. 2007 Page(s):2894 – 2901

[6]   A. Rida, L. Yang, R. Vyas, S. Basat, S. Bhattacharya, and M. M. Tentzeris "Novel Manufacturing Processes for Ultra-Low-Cost Paper-Based RFID Tags With Enhanced "Wireless Intelligence"" Proc. Of the 57th IEEE-ECTC Symposium, pp. 773-776, Sparks, NV, June 2007.

[7]   L.Yang, and M.M. Tentzeris, "3D Multilayer Integration and Packaging on Organic/Paper Low-cost Substrates for RF and Wireless Applications" ISSSE '07. International Symposium on Signals, Systems and Electronics, 2007. July 30 2007-Aug. 2 2007 Page(s):267 – 270

[8]   M.M. Tentzeris, L. Yang, A. Rida, A. Traille, R. Vyas, and T. Wu, "RFID's on Paper using Inkjet-Printing Technology: Is it the first step for UHF Ubiquitous "Cognitive Intelligence" and "Global Tracking"?" RFID Eurasia, 2007 1st Annual 5-6 Sept. 2007 Page(s):1 – 4

[9]   A. Rida, R. Vyas, S. Basat, A. Ferrer-Vidal, L. Yang; S. Bhattacharya, and M.M. Tentzeris, "Paper-Based Ultra-Low-Cost Integrated RFID Tags for Sensing and Tracking Applications" Electronic Components and Technology Conference, 2007. 57th May 29 2007-June 1 2007 Page(s):1977 – 1980

[10]   M.M. Tentzeris, L. Yang, A. Rida, A. Traille, R. Vyas, and T. Wu, "Inkjet-Printed RFID Tags on Paper-based Substrates for UHF "Cognitive Intelligence" Applications" IEEE International Symposium on Personal, Indoor and Mobile Radio Communications, 3-7 Sept. 2007 Page(s):1 – 4

[11] A. Rida, L Yang; R. Vyas, S. Bhattacharya,.and M.M. Tentzeris, "Design and integration of inkjet-printed paper-based UHF components for RFID and ubiquitous sensing applications" IEEE Microwave European Conference, pp:724-727, Oct 2007

[12] G. Zou, H. Gronqvist, J.P. Starski, and J. Liu, "Characterization of Liquid Crystal Polymer for High Frequency System-on-a-Package Applications," IEEE Trans. Advanced Packaging, vol. 25, no. 4, pp. 503-508, November 2002.

[13] D. Thompson, O. Tantot, H. Jallageas, G. Ponchak, M. M. Tentzeris, J. Papapolymerou, "Characterization of LCP material and transmission lines on LCP substrates from 30 to 110GHz," IEEE Trans. Microwave Theory and Tech., vol. 52, no. 4, pp. 1343-1352, April 2004.

[14] Dimatix datasheet http://www.dimatix.com/files/DMP-2831-Datasheet.pdf, date visited: Sep 2008

[15] A. Pique, and D. B. Chrisey, "Direct-write Technologies for Rapid Prototyping Applications", Academic Press, 2002. International Standard Book Number: 0-12-174231-8.

[16] M. Carter, J. Colvin, and J. Sears, "Characterization of conductive inks deposited with maskless mesoscale material deposition", TMS2006, Mar. 12-16, San. Antonio, Texas, USA

[17] Fujifilm Dimatix Inc, Piezo-electric Ink-jet Print-Heads, HTTP: http://www.dimatix.com/markets/electronics.asp, date visited: Dec 2008

[18] O. Azucena, J. Kubby, D. Scarbrough, and C. Goldsmith, "Inkjet printing of passive microwave circuitry" IEEE MTT-S International Microwave Symposium Digest, pp: 1075-1078, June 15-20

[19] C. Balanis, "Antenna Theory, Analysis and Design," third edition, John Wiley & Sons, Inc., Publication.

[20] R.A. Burberry, "VHF and UHF Antennas," IEE Electromagnetic Waves Series 35. Peter Peregrinus Ltd. On behalf of the Institution of Electrical Engineers.

[21] Texas Instrument, "UHF Gen2 Strap RI-UHF-STRAP-08," Data Sheet, October 2006.

[22] S.D. Kulkarni, R.M. Boisse, and S.N. Makarov, "A Linearly-Polarized Compact UHF PIFA with Foam Support", Department of Electrical Engineering, Worcester Polytechnic Institute.

[23] P.V. Nikitin, S. Rao, S.F. Lam, V. Pillai, and H. Heinrich, "Power Reflection Coefficient Analysis for Complex Impedances in RFID Tag Design" IEEE Transactions on Microwave Theory and Techniques, VOL. 53, Sep. 2005.

[24]   J. Siden, M.K. Fein, A. Koptyug, and H,-E, Nilson, "Printed antennas with variable conductive ink layers" IET Microwaves, Antennas and Propagation, Volume 1, Issue 2, pp: 401-407, April 2007

[25]   UHF RFCPUs on Flexible and Glass Substrates for Secure RFID Systems, Kurokawa, Y.; Ikeda, T.; Endo, M.; Dembo, H.; Kawae, D.; Inoue, T.; Kozuma, M.; Ohgarane, D.; Saito, S.; Dairiki, K.; Takahashi, H.; Shionoiri, Y.; Atsumi, T.; Osada, T.; Takahashi, K.; Matsuzaki, T.; Takashina, H.; Yamashita, Y.; Yamazaki, S.; Solid-State Circuits, IEEE Journal of Volume 43, Issue 1, Jan. 2008 Page(s):292 – 299

[26]   UHF RFCPUs on Flexible and Glass Substrates for Secure RFID Systems Kurokawa, Y.; Ikeda, T.; Endo, M.; Dembo, H.; Kawae, D.; Inoue, T.; Kozuma, M.; Ohgarane, D.; Saito, S.; Dairiki, K.; Takahashi, H.; Shionoiri, Y.; Atsumi, T.; Osada, T.; Takahashi, K.; Matsuzaki, T.; Takashina, H.; Yamashita, Y.; Yamazaki, S.; Solid-State Circuits Conference, 2007. ISSCC 2007. Digest of Technical Papers. IEEE International 11-15 Feb. 2007 Page(s):574 – 575

[27]   L. Yang, S. Basat, A. Rida, and M.M. Tentzeris, "Design and Development of Novel Miniaturized UHF Tags on Ultra-low-cost Paper-Based Substrates" IEEE Asia Pacific Microwave Conference, pp: 1493-1496, Dec 2006

[28]   A. Rida, L. Yang, and M. M. Tentzeris, "Design and characterization of novel paper-based inkjet-printed UHF antennas for RFID and sensing applications" Procs. of the 2007 IEEE-APS Symposium, pp2749-2752, Honolulu, HI, July 2007

[29]   S. Bhattacharya, M.M. Tentzeris, L. Yang; S. Basat, A. Rida, "Flexible LCP and Paper-based Substrates with Embedded Actives, Passives,and RFIDs" International Conference on Polymers and Adhesives in Microelectronics and Photonics, 2007. Jan. 16 2007-Page(s):159 – 166

[30]   J. D. Griffin, G. D. Durgin, A. Haldi, and B. Kippelen, "RF Tag Antenna Performance on Various Materials Using Radio Link Budget," IEEE Antennas and Wireless Propagation Letters, Dec 2006

[31]   A. Ferrer-Vidal, A. Rida, S. Basat, L. Yang, and M.M. Tentzeris, "Integration of sensors and RFIDs on ultra-low-cost paper-based substrates for wireless sensor networks applications" IEEE Workshop on Wireless Mesh Networks, 2006 Page(s):126 – 128